Gjermund Kvåle Jordheim

A characterization of the somatostatin expressing cell population in the lateral entorhinal cortex of the mouse

Master's thesis in Neuroscience
Supervisor: Bente Jacobsen, MSc
Trondheim, June 2016

Norwegian University of Science and Technology
Faculty of Medicine
Kavli Institute for Systems Neuroscience / Centre for Neural Computation

NTNU
Norwegian University of
Science and Technology

Abstract

The lateral entorhinal cortex is a part of the parahippocampal region, and has received attention for being involved in object and object characterization task, hence conveying non-spatial input to the hippocampal formation. In order to fully comprehend the functional role of the lateral entorhinal cortex, an important step is to understand the function of its local micro circuitry. Interneurons have been strongly implemented in the functioning of cortical networks. However, little is known concerning the interneurons in the lateral entorhinal cortex

The aim of this thesis was to characterize the distribution of somatostatin cells in the lateral entorhinal cortex, and to look at their monosynaptic inputs. For the distribution analysis we injected an adeno-associated helper virus into the lateral entorhinal cortex of somatostatin-Cre mice. In our monosynaptic tracing experiments, we injected both adeno-associated helper virus and a G-deleted rabies virus into the lateral entorhinal cortex in our transgenic mouse line. We tested several viral strategies to optimize the viral tracing protocol. Cresyl Violet stained sections were used to delineate brain areas. Viral tracers were visualized either by the expression of fluorescent proteins or immunohistochemically enhanced with AlexaFluor dyes. The tissue was subsequently analyzed by using traditional microscopical techniques.

After testing several viral injections strategies, we found that the most optimal strategy involved separate injections of virus, separated by a sufficient incubation period which serves to ensure the framework for viral transport. The results from the monosynaptic viral tracing experiments showed that the somatostatin cells in the lateral entorhinal cortex have a strong intrinsic connectivity within the LEC, but also receive a substantial amount of input from extrinsic sources. Our distribution analysis showed that the majority of somatostatin cells are situated in deeper layers of the lateral entorhinal cortex, and that they are evenly distributed throughout the dorsoventral axis.

Acknowledgments

The work presented in this thesis was performed at the Kavli Institute for Systems Neuroscience for Neural Computation at the Norwegian University of Science and Technology (NTNU), under the supervision of Bente Jacobsen.

First of all, to my supervisor Bente, thank you for always being really helpful, patient and for guiding me through my project. I would also like to thank you, Menno, for giving me this opportunity to work in your lab. To Bruno, thanks for your assistance in the lab and all the chats, jokes and laughs I have had over by the coffee machine. And to the rest of the Witter Group, thank you for always being supportive.

Further, I would like to thank my family, friends and Hanna for supporting me through my studies. Finally, I would like to thank my friend, Martin, for both the academic and highly un-academic discussions we have had over the past year.

Table of Contents

List of abbrivations

- **PHR –** Parahippocampal region
- **HF –** Hippocampal formation
- **EC –** Entorhinal Cortrex
- **LEC –** Lateral Entorhinal Cortex
- **MEC –** Medial Entorhinal Cortex
- **IN –** Interneuron
- **L -** Layer
- **Pir –** Piriform Cortex
- **PRh –** Perirhinal Cortex
- **HDB –** Horizonal limb of the diagonal band
- **VDB –** Vertical limb of the diagonal band
- **CA –** Cornu Ammonis
- **Sub –** Subiculum
- **GABA -** y-amino butyric acid
- **MC –** Martinotti Cell
- **PV –** Parvalbumin
- **SOM –** Somatostatin
- **VIP –** Vasoactive Intestinal Peptide
- **RABV –** Rabies Virus
- **AAV –** Adeno-associated virus
- **EnvA –** Avian ASLV typa A envelope protein
- **TVA –** T Virus receptor A
- **PFA –** Paraformaldehyde
- **DMSO –** Dimethyl Sulfoxide
- **Tris-HCl –** Tris Hydrochloride Buffer
- **PB –** Phosphate Buffer
- **IHC –** Immunohistochemistry
- **PBT –** Phosphate Buffer + 1% Trx
- **RT –** Room temperature
- **GFP –** Green Fluor Protein
- **NGS –** Natural Goat Serum
- **HA –** Human influenza hemagglutinin
- **Tub –** Olfactory Tubercule
- **AuC –** Auditory Cortex
- **SSC –** Somatosensory cortex
- **CL –** Contralateral
- **AIP –** Insular cortex
- **Amy** – Amygdala
- **MSC –** Medial septum complex
- **Cl –** Claustrum
- **Den –** Dorsal endopiriform nucleus
- **ATA –** Amygdalostriatal transition area
- **Th –** Thalamus
- **MS –** Medial septum (nucleus)

1. Introduction

The role of the parahippocampal region (PHR) and the adjacent hippocampal formation (HF) (figure 1) has for long enthralled neuroscientists, ever since Ramon y Cajal first described its anatomy in 1881 (Golgi et al., 2001). As the anatomy of the PHR and the HF seems to be largely preserved across species, animal models are well suited for interpreting the role of the PHR and HF in humans (Amaral et al., 2007). The HF and PHR have for long been associated with learning and memory (Scoville and Milner, 1957), however the discovery of place cells in 1971 suggested that these areas were fundamentally involved in spatial navigation as well (O'Keefe and Dostrovsky, 1971). Lately these regions have received a lot of attention after the discovery of grid cells in the entorhinal cortex (EC) (Hafting et al., 2005), but the EC is also known to be involved in other non-spatial tasks (Tsao et al., 2013).

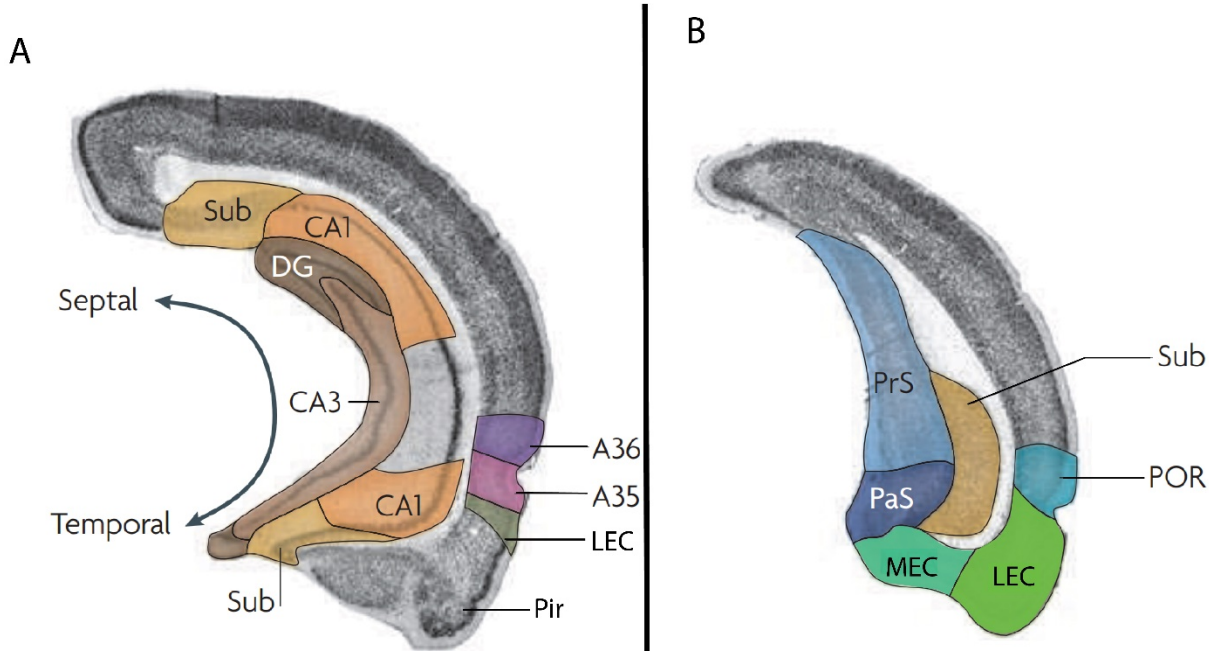

Figure 1: The hippocampal and parahippocampal region. Coronal sections of the rat brain, showing the different structures of the hippocampal and parahippocampal regions. Abbrivations relavant for this thesis are found on page xi. Adapted and modified from (van Strien et al., 2009).

The EC is a part of the PHR and is situated in the caudal portion of the rodent brain. The EC is perceived as the nodal point in the exchange of information between the HF the (neo)cortex, and is thus thought to have a central role in cortico-hippocampal interactions (Kerr et al., 2007). The name 'entorhinal' is derived from the ECs position within the brain, being partially enclosed by the rhinal sulcus (Canto et al., 2008). The EC consists of two subregions known as the medial entorhinal cortex (MEC) and the lateral entorhinal cortex (LEC). Besides having similar names, the two regions are different from each other when it comes to their cytoarchitecture and connectivity with other brain areas (Insausti et al., 1997, Knierim et al., 2014).

The major differences related to the input sources of the two structures, are likely to contribute to their functional dichotomy. Due to these differences, the LEC and the MEC have been thought to be involved in two functional distinct streams of input to the HF (Deshmukh and Knierim, 2011). The MEC has been suggested to be involved in a so-called "where" stream in to the HF, as it is connected to areas that provide spatial- and movement-related inputs. Many different types of spatially modulated cells have been recorded in the MEC, including grid cells, border cells and head direction cells (Taube and Muller, 1998, Fyhn et al., 2004, Hafting et al., 2005)**.** The LEC, on the other side, is part of the "what" stream, with neurons responding to olfactory and tactile information, amongst other things. Object and object trace cells are among the different functional cell types reported in the LEC, and the LEC is thought to convey non-spatial information to the HF, and to be involved in the characterization of objects (Figure 2) (Eichenbaum et al., 2007, Tsao et al., 2013, Knierim et al., 2014)

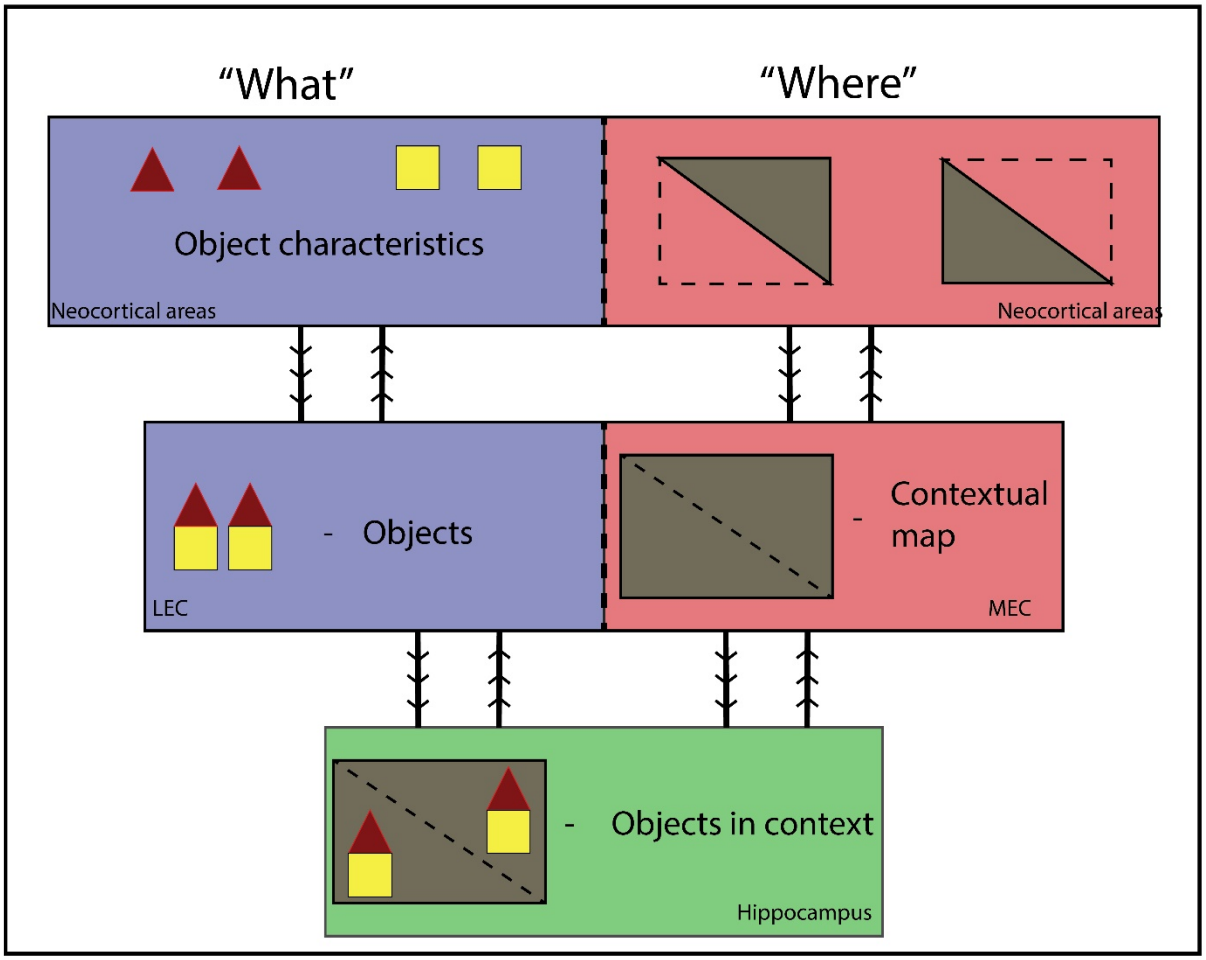

Figure 2: Functional differences between the LEC and the MEC. Non-spatial neocortical inputs from the so-called "what" stream targets the LEC and convey information regarding object characteristics, such as smell, texture and sound. Spatial input from the "where" stream preferentially target the MEC. The LEC and the MEC subsequently project to the HF where the "what" and "where" stream converge and make up a representation of objects in a spatial context.

It has been speculated that some of the spatial properties of MEC are the result of computations arising in the internal network, thus it would be conceivable that the MEC and the LEC differ in their internal network connections as well. Earlier reports have indicated that there are differences related to the intrinsic connectivity of the LEC and the MEC (Dolorfo and Amaral, 1998). However, studies characterizing major differences in the intrinsic connectivity of these two regions are sparse. In particular, very little is known about

the local connections of interneurons (IN), which have been strongly implicated in the functioning of cortical networks (Markram et al., 2004).

This thesis is primary concerned with input projections to INs in the LEC, hence this will be the main focus in the following sections.

1.1 Lateral entorhinal cortex

The LEC makes up the rostrolateral part of the EC which is situated in the ventrocaudal convexity of the rat's cerebral hemisphere. As some of its adjacent structures, the LEC is considered to be a part of the so-called periallocortex, a transitional zone between the neocortex and the allocortex. The LEC is generally divided in to six layers, where four of the layers (II, III, V and VI) can be considered as cellular, while layer (L) I and LIV can be considered to be acellular (Cappaert et al., 2015).

1.1.1 Intrinsic organization of the lateral entorhinal cortex

LI is a relatively cell free layer and consist mainly of fibers that are oriented transversely along the surface of the pia (Witter and Amaral, 2004). The cells that are situated in this layer are mainly INs, but a few glutamatergic cells are present here as well (Miettinen et al., 1997, Wouterlood and Pothuizen, 2000, Canto and Witter, 2012b). LII mainly consists of medium- and large-sized principal cells, and the cells in LII of the LEC may form islands, which are small areas of higher cell density (Insausti et al., 1997, Witter and Amaral, 2004). Fan cells have been shown to be the main excitatory cell type in the layer, and multiple classes of INs have been observed here as well (Canto and Witter, 2012b). LIII makes up a layer of cells having various shapes and sizes (Witter and Amaral, 2004). Principal cells in LIII are a relatively homogenous group of pyramidal cells (Tahvildari and Alonso, 2005). LIV is also referred to as the lamina dissecans, and sporadically principal cells are located in this layer (Canto et al., 2008). However, this layer is generally considered as an acellular layer mainly consisting of INs and neuropil (Witter and Amaral, 2004). Large pyramidal cells make up the majority of cells in LV of the LEC, and LV is considered as quite homogenous throughout the entire EC, with no major differences in architecture between the LEC and the MEC (Canto and Witter, 2012a, Canto and Witter, 2012b) LVI consists of neurons that

together constitute a fairly heterogeneous population of cells, and cell density typically decreases towards the white matter (Witter and Amaral, 2004). Principal cells situated in LVI have been reported to distribute their dendrites in LV and LVI. Their axon collaterals typically extend superficially from the somata in LVI to LV and LIII(Canto and Witter, 2012a).

1.1.2 Afferents to the lateral entorhinal cortex

The LEC and the MEC are often referred to as the major input and output structures of the HF (Canto et al., 2008). The LEC receives a lot of input from multiple cortical and subcortical structures, including a fair amount of input from the HF. The following section gives a short summary of the major inputs to the LEC.

(Neo) cortical input

The Piriform cortex (Pir) exhibits the strongest extrinsic connection to the LEC, and is reported to constitute approximately 1/3 of the total (neo)cortical input to the area (Burwell and Amaral, 1998). The projections from the Pir preferentially terminate in LI of the LEC where they make synapses on distal dendrites of principal cells in LII and LIII (Wouterlood and Nederlof, 1983). About 10% of the cortical afferents to the LEC arise from structures situated in frontal cortical areas (Burwell and Amaral, 1998). A large input to the LEC is also seen from the insular cortex, which preferentially targets the deeper layers of the LEC (Mathiasen et al., 2015). The combined input from the perirhinal cortex (PRh), the postrhinal and the ventral temporal association cortices make up approximately 25% of the total cortical input to the LEC, with the PRh input being strongest of the three (Burwell and Amaral, 1998).

Subcortical input

The endopiriform nucleus and the piriform transition area form the strongest subcortical projections to the LEC, both are areas involved in olfactory processing (Kerr et al., 2007). There is also a moderate projection from the medial septal complex to the LEC, particularly cells within the horizontal limb of the diagonal band (HDB) have been found to distribute

fibers to the LEC where they preferentially target LII and LIV (Alonso and Kohler, 1984). The amygdala is another subcortical structure that has been found to send moderate projections to the LEC. Inputs from the different nuclei of the amygdala have been reported to preferentially terminate in LIII and LIV (Pitkanen et al., 2000). Amygdaloid nuclei that are involved in olfaction have been reported to be particularly prominently connected to the LEC (Kerr et al., 2007). Strong input to the LEC is also seen from the ventral parts of the claustrum, and afferents from the claustrum preferentially target deeper layers of the LEC (Behan and Haberly, 1999, Kerr et al., 2007).

Hippocampal input

The LEC is more strongly connected to the ventral parts of the HF than to the dorsal parts (Agster and Burwell, 2013). With regards to hippocampal structures it seems that more than half of the afferents from the HF to the LEC are from cells situated in the cornu ammonis (CA) 1 (Agster and Burwell, 2013). Cells in the Subiculum (Sub) account for approximately a quarter of the inputs to the LEC. These two regions make up the two major outputs regions from the HF to the LEC. (Agster and Burwell, 2013). Hippocampal input to the LEC has been reported to primarily target deeper layers, but sparse fiber also terminate in LIII (Naber et al., 2001, Kloosterman et al., 2003).

1.2 Interneurons

The brain is made up of a diverse population of neurons that all have their distinct functions. The largest subpopulation of neurons is formed by excitatory principal cells, which make up approximately 80% of the neuronal population. A smaller subgroup of neurons in the brain is the so-called INs, which are mainly inhibitory and express the neurotransmitter y-amino butyric acid (GABA). The INs are an immensely diverse cell group with regards to morphological, physiological and molecular properties (Markram et al., 2004, Yuste, 2005). This great diversity of GABAergic INs are thought to play an essential role in the cortical micro circuitry, as they have been found to have different roles in controlling the different aspects of the principal cells' activities. GABAergic INs have also been found to be involved in the generation of cortical rhythms (Markram et al., 2004, Rudy et al., 2011). Through their

diverse functions, the INs are able to regulate the information flow in the different neural networks and in this way exert control over the spatiotemporal processing of information in the brain (Rudy et al., 2011).

1.2.1 Interneurons in a (neo)cortical micro circuit

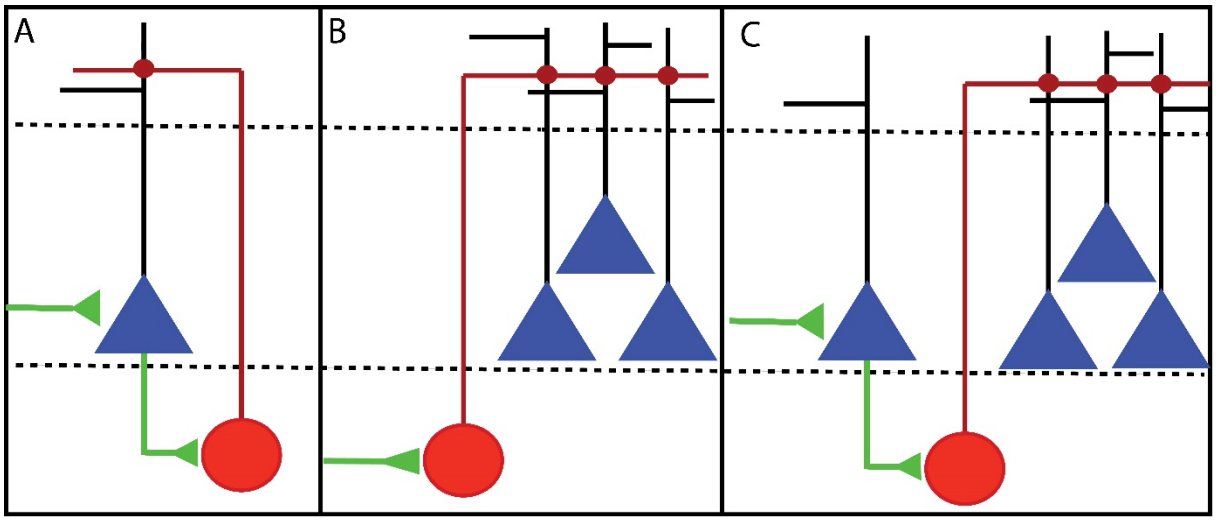

Figure 3: Feedback-, feedforward- and lateral inhibition: **A:** Feedback inhibition, a principal cell (blue) excites an IN (red) within the same cortical area. The INs project back and inhibit surrounding principal cells. **B:** Feedforward inhibitory loop, extrinsic input directly targets an IN within a cortical area, which in turn projects to the principal cells within the same cortical area to modulate their activity. **C:** Lateral Inhibition, a principal cells contacts indirectly dampens the activity of surrounding principal cells in interaction with an IN. Excitatory fibers are indicated by green lines. Inhibitory fibers are indicated by red lines. Dendrites are indicated by black lines.

In an inhibitory network, INs have been shown contribute to both feedback, feedforward and lateral inhibition mechanisms (Buzsaki, 1984, Markram et al., 2004, Isaacson and Scanziani, 2011). For feedback inhibition, increased firing of a principal cell leads to increased firing in local INs, which in turn project back and decrease the activity of the principal cell. Feedback inhibition can thus be viewed as a self-regulatory mechanism aiming to ensure stability within the (neo)cortical network (Figure 3A) (Isaacson and Scanziani, 2011). Feedforward inhibition is a mechanism where an afferent increases the activity in an IN which in turn decreases the activity of principal cells (Figure 3B). As feedforward

inhibitory systems are known to be more unstable, Buzaki claims that both feedback and feedforward inhibition needs to be present in order to establish a stable networks (Buzsaki, 1984).The last form for inhibition, lateral inhibition, has been viewed as a mechanism where local principal cells can dampen the activity of other surrounding principal cells by recruiting local INs (Figure 3C), thus increasing their single-to-noise ratio (Silberberg and Markram, 2007, Berger et al., 2010, Isaacson and Scanziani, 2011)

1.2.2 Classification of interneurons

Due to the diversity of INs, there has been a need to classify the different interneuronal subpopulations. The subpopulations of INs may be separated from each other morphologically, electrophysiologically or based on expression certain of biochemical markers. In the following section I will focus on the biochemical and morphological classification (Markram et al., 2004, Ascoli et al., 2008, Rudy et al., 2011).

Interneuron morphology

Morphologically, INs are typically classified by looking at their axons. The axonal morphology has been found to be correlated with both the developmental origin and synaptic physiology of the INs (Ascoli et al., 2008). The different morphological subgroups typically target distinct regions of the principal cells, and they can be split into axon-targeting, soma- and proximal dendrite-targeting, dendrite-targeting, and dendrite and tuft-targeting subgroups (Markram et al., 2004). Of the soma- and proximal dendrite-targeting INs, the basket cells are the most prominent. Basket cells make up approximately half of the IN population in the (neo)cortex and they are characterized by their axons forming basket-like structures surrounding the somata of principal cells (Wang et al., 2002, Markram et al., 2004). Chandelier cells target the axon initial segment of their synaptic targets (Markram et al., 2004). INs that are mainly dendrite-targeting have been identified as bipolar cells, double bouquet cells and bitufted cells, and also as Martinotti cells (MCs) (Markram et al., 2004, Druga, 2009).

Biochemical markers

The diversity that different subpopulations of INs show can also be associated with the expression of specific molecular markers. INs can be split into three major non-overlapping groups based on their expression of three different markers; the calcium-binding protein parvalbumin (PV), the ionotropic serotonin receptor 5HT3a and the neuropeptide somatostatin (SOM) (Lee et al., 2010, Rudy et al., 2011). However, the 5HT3a group probably contains several subgroups including a group of cells that express the neuropeptide vasoactive intestinal peptide (VIP) (Lee et al., 2010, Rudy et al., 2011). The different biochemical groups are associated with several morphological subgroups, but certain morphological features are more commonly found within each molecular class. PV cells are most often basket cells or chandelier cells, SOM cells are often MCs, and VIP expressing neurons are often cells with bipolar or bitufted morphologies (Rudy et al., 2011).

1.2.3 Martinotti cells

MCs are found in LII- VI of the neocortex, and are estimated to make up approximately 15% of the total IN population (Druga, 2009). MCs are the largest group of SOM cells, and approximately 70% of all SOM cells have a MC morphology. Typically, the dendrites are oriented vertically and project into adjacent layers, giving them a bi-tufted appearance. Even though their dendritic arborizations are quite characteristic, the axonal configuration of the MCs make them easy to distinguish from other INs. The axons of MCs project superficially and densely innervate LI tangentially to the pial surface, often covering distances up to a millimeter. Due to these extensive axonal arborizations it is believed that MCs can coordinate activity across cortical columns (Wang et al., 2004, Jiang et al., 2015). The MCs seems to project to nearly every neuronal types within its axonal tree, and all contacts seem to be of equal strength. The input to MCs seem to consist of local afferents from principal cells and INs (Jiang et al., 2015).

1.2.4 Somatostatin expressing interneurons in the lateral entorhinal cortex

Little is known about the SOM expressing IN population in the LEC. There are still many questions related to their function, morphology and laminar distribution. Earlier studies have characterized the distribution of SOM cells, but the results are conflicting. Köhler and Chan-Palay reported that the SOM cells were most abundant in deeper layers (Kohler and Chan-Palay, 1983). However, Wouterlood and Pothuizen reported that most SOM positive cells were present in superficial layers, even though a substantial amount of the cells were located in LV and LVI (Wouterlood and Pothuizen, 2000). If we look to the (neo)cortex and other region in the PHR, SOM cells are mainly be located in deeper layers (Morrison et al., 1983)

1.3 Monosynaptic tracing with pseudotyped G-deleted rabies virus

Genetically engineered viral vectors have proven to be efficient tools for investigating the anatomical connectivity of specific neuronal subpopulations. Thus, giving insight in to the cell type specific circuits of the brain. Monosynaptic retrograde tracing techniques are relatively new in the neuroanatomical tool box, and they are carried out with the use of a helper virus and a specialized rabies virus (RABV) in specifically engineered transgenic mouse lines (Callaway and Luo, 2015).

1.3.1 Cre-driver lines

Mouse lines expressing Cre recombinase in subpopulations of cells are readily available, and the Cre recombinase system is a way to flexibly alter the gene expression in these groups of cells (Callaway and Luo, 2015). Cre recombinase is an enzyme that catalyzes recombination located between two DNA recognition sites, so-called loxP sites. Two LoxP sites are situated within the DNA, flanking a gene of interest, thus separating the recombination sequence from the rest of the DNA. By catalyzing loxP, the recombination sequence flanked by loxP, is cut out of the DNA. By a proper insertion of a loxP-flanked stop sequence between a promoter and a transgene in the DNA, the stop sequence can be cut out of the DNA when Cre recombinase is present. This way, only cells expressing Cre recombinase are able to remove the stop sequence from the DNA and hence expressing the transgene (Nagy, 2000).

Cre-dependent expression of genes introduced by viral vectors can be used as a port of a monosynaptic tracing experiment in order to target specific cell groups as the starter population.

1.3.2 Adeno-associated virus

Adeno-associated virus (AAV) is part of the parvovirus family and is one of the smallest DNA viruses. AAV viruses are commonly used for gene therapy, as they are well suited as viral vectors and are reported to have a low level pathogenicity (Grieger and Samulski, 2005, Daya and Berns, 2008). In order to target the monosynaptic tracing to a particular group of starter cells Cre-dependent AAV helper viruses are used to provide the cells with the genes needed for the rabies to be able to infect and transport from the starter population. A typical helper virus carries genes coding for an avian tumor virus Receptor A (TVA) receptor, a G-protein and also a protein tag (Ginger et al., 2013)**.** The TVA receptor is a receptor not naturally found in neurons, and a rabies virus can be engineered to carry the right surface proteins needed to bind to this receptor and infect the cells, thus giving a restricted rabies infection (Federspiel et al., 1994). The G-protein is a cell-adhesion protein that is needed for the rabies to be able to transfer monosynaptically to the presynaptic cells of the primary infected population (Mazarakis et al., 2001). The protein tag carried by the AAV helper virus is there to be able to detect which cells were the starter cells for the rabies infection.

1.3.3 Rabies virus

RABV is a virus in the *rhabdoviridae* family, and its wild-type variety causes severe and deadly infections in both humans and animals (Ghanem and Conzelmann, 2016). RABV infects the nervous system and is known to spread retrogradley from cell to cell and exploit the cell machinery to replicate and ensure further spread (Schnell et al., 2010). The retrograde transport mechanism of the RABV is thought to be mediated by the G-protein that coats the outer membrane (Schnell et al., 2010). The inherent properties of RABV may be exploited for use in neuroanatomical tracing. By altering some of its wild-type properties, the infection of the virus, and its subsequent synaptic transport, may be restricted. In monosynaptic tracing experiments, pseudotyped RABV with a deleted G-protein is used. With no genes coding for G-proteins in its genome, the RABV is unable to infect cells (Schnell

et al., 2010, Ghanem and Conzelmann, 2016). By pseudotyping the RABV, it is possible to express proteins on its' surface that are specific for receptors that have been expressed due to the helper virus described above. In mammals, RABV is usually coated with the envelope protein from an avian ASLV type A (EnvA), which interacts with a TVA receptor that can be conditionally expressed in certain cell types (Callaway and Luo, 2015).

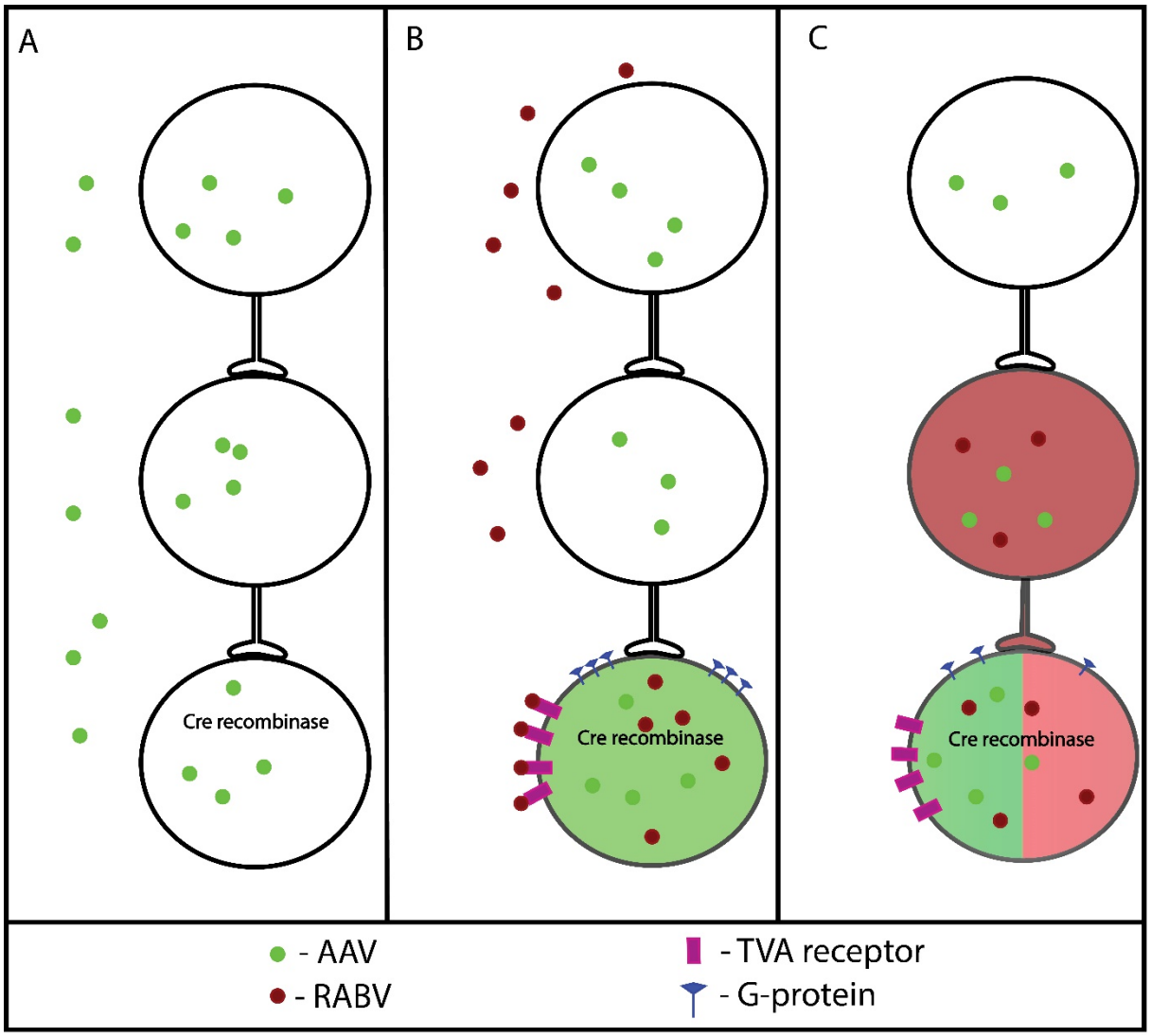

Figure 4: Monosynaptic retrograde tracing. A: An AAV virus is injected into an area of interest where target cells express Cre recombinase. **B:** When the cell has expressed the proteins that the AAV helper codes for, it can be infected by the pseudotyped G-deleted RABV. As the AAV virus carries a gene coding for a protein tag, the starter cell can be recognized. **C:** The G-deleted RABV will replicate in the infected cells, and receive G-protein due to the genes of the AAV helper virus. This will make the RABV able to spread to presynaptic cells. The RABV carries a fluorescent marker that makes it possible to recognize.

This means that RABV only can infect cells expressing the TVA receptor, by use of a helper virus the same cells can be made to express the G-protein needed for the rabies virus to travel in a retrograde manner. As only a specific subset of cells express this protein, the virus can only be transported one synapse back from the primary infected cells, this ensures monosynaptic retrograde tracing.

1.3.4 Monosynaptic tracing

When combining the properties of Cre recombinase, the helper virus AAV and the pseudotyped G-deleted RABV virus, it is possible to trace the monosynaptic inputs to the Cre-expressing starter cells. By choosing an appropriate transgenic mouse line Cre recombinase is present in the desired subpopulation of cells. When the AAV helper is injected it will infect all cells (Figure 4A), but only express its “payload” in cells expressing Cre recombinase (Figure 4B). Then, the pseudotyped G-deleted RABV is injected and it can only infect cells expressing the TVA receptor on their cell surface (Figure 3B). Once the RABV has infected the cell it will start to replicate and although the ability to generate G-protein has been removed from its genome, the AAV virus has provided the cell with the genes to produce the G-protein needed by the RABV in order to be transported to presynaptic cells. The RABV is able to jump one synapse and infect the presynaptic neuron but is unable to spread further because of the lack of G-protein in the presynaptic cell (Figure 4C) (Wall et al., 2010, Callaway and Luo, 2015).

1.4 Aim

In this thesis I aim to characterize the distribution of SOM expressing cells in the LEC, and to identify the main inputs to these cells through retrograde monosynaptic tracing. In addition, I will determine the specificity of the Ssttm2.1(cre)Zjh/J transgenic mouse line and test several viral injection strategies in order to optimize the retrograde monosynaptic tracing protocol.

2. Materials and methods

2.1 General methods

2.1.1 Animals

This study used 11 animals of both genders of the SST-cre (Ssttm 2.1(cre)Zjh/Jax) transgenic mouse line from the Jackson laboratories, all weighing between 20 and 35 g. Animals were kept in a standardized environment (12hr reversed day/night cycle, 21 ± 1°C, 60% RH) with *ad libitum* access to food and water. All animals used were raised and handled according to regulations and laws provided by Forsøksdyrutvalget (The Norwegian Research Authority).

2.1.2 Anaesthesia and analgesia

Prior to surgery, all animals were weighed and anesthetized with isoflurane (air flow: 1L/min, 4% isoflurane) in an induction chamber. At the start of the surgery, the mice were given subcutaneous injections with Rimadyl (50 mg/ml, 1:50 dilution, 5 mg/kg) and Temgesic (0.3 mg/ml, 1:10 dilution, 0,05-0.1 mg/kg). The local anesthetic Marcain (2.5 mg/ml, 1:5 dilution, 1 mg/kg) was injected subcutaneously along the skull prior to incision. During surgery, the isoflurane was administered through a surgical mask, and the level of anesthesia was monitored and adjusted throughout the surgery (airflow 1L/min, 1-2% isofluorane). The depth of anesthesia was examined by observing breathing frequency, and at the beginning of the surgery by testing pinch reflexes. Rimadyl was also administered the following day to relieve any postoperative pain. A full list of all the solutions and chemicals used in this thesis can be seen in appendix IV and V.

2.1.3 Surgical procedure

After being anesthetized, animals were mounted and fixed in a stereotaxic surgical frame (Kopf, Tujunga, USA). In order to fixate the animal's head position, ear bars were positioned in the animal's external ear cavity. The surgical area was shaved and disinfected with ethanol and iodine. An incision of the skin was made over the midline of the skull. The periost was

scraped to the sides using a scalpel and cotton swabs. This revealed the two coronal sutures and the intersections with the midsagittal one, called lambda (posterior) and bregma (anterior), which were used as reference points in order to align the skull in the horizontal plane. In order to reveal the sagittal sinus, the skull was thinned slightly at the midline. The lambda and bregma (Figure 5), as well as the transverse and sagittal sinuses, served as reference points to calculate coordinates for tracer injections. Viral tracers were injected into the LEC with a Hamilton syringe (Hamilton Company, USA). The stereotaxic coordinates for all the injections were as follows: *4.5 mm mediolateral from the sagittal sinus; -3.2 mm dorsoventral from the dura mater; 2.0 mm rostral from the transvers sinus, measured 3.0 mm lateral from the sagittal sinus.* After the syringe had been lowered into the LEC, we waited for two minutes to allow the tissue surrounding the syringe to retract to its original form. The virus was injected over a period of 10-15 minutes, depending on the volume of the injection. After the injection, the syringe was kept in place for 10-15 minutes to ensure that the virus had sufficient time to diffuse into the surrounding tissue.

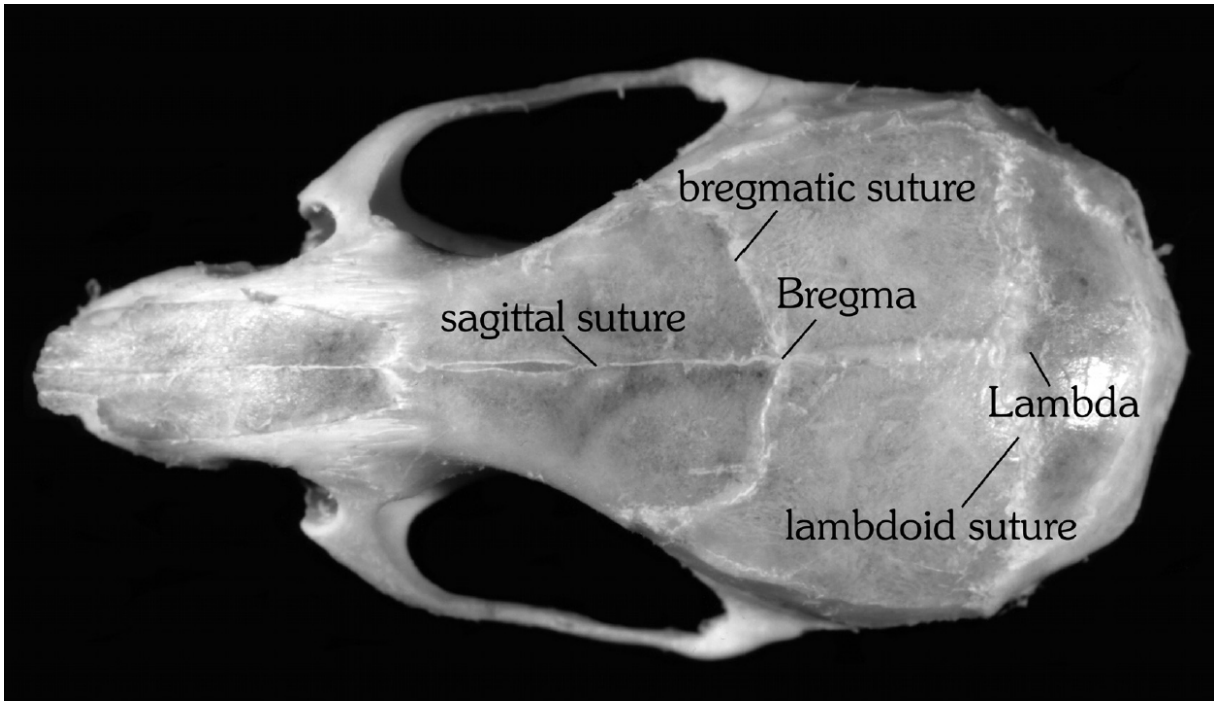

Figure 5: Skull diagram: A picture of the dorsal surface of the mouse skull, showing the reference point Bregma and Lambda (Figure adapted from Franklin and Paxinos (2007).

Finally the syringe was slowly removed from the brain. A more detailed protocol of the surgeries can be found in appendix II. After the surgery was completed, the skin and skull

were cleaned with saline. The incision was sutured and rinsed with saline before the animal was placed in a heat chamber for recovery. When the animal woke up, and regained normal functions, it was placed in its home cage and monitored the following days. All surgeries were performed by my supervisor Bente Jacobsen.

2.1.4 Perfusion

Before tissue collection, the animals were weighed and anesthetized with isoflurane. When the animals were sufficiently anesthetized, they were given an intraperitoneal overdose with pentobarbital (100 mg/mL, 30-90 mg/kg) (Sanofi Sante, Maassluis, The Netherlands). After making sure that all reflexes and pain responses were absent, the animals were transcardially perfused. The animal's chest cavity was cut open with scissors, such that the heart was exposed. A needle (27 gauge), attached to a peristaltic pump (World Precision Instruments, USA), was inserted into the left ventricle of the heart, while the right atrium was subsequently cut open with scissors. A ringer solution was then pumped through the cardiovascular system until all the blood had been eluted. The ringer solution was then exchanged with day fresh 4% paraformaldehyde (PFA) in a 0.125 M phosphate buffer for fixation. When the tissue was sufficiently fixed, the brain was carefully removed from the skull and placed in a brain cup containing 4% PFA for an overnight post-fixation at 4°C. The day after, the brain was transferred to another brain cup containing dimethyl sulfoxide (DMSO) (Phosphate buffer, 2% dimethyl sulfoxide and 20% glycerol) for cryoprotection. The brains were then stored in a refrigerator at 4°C until sectioning. A full list of all the solutions and chemicals used in this thesis can be seen in appendix IV and V.

2.1.5 Sectioning

For sectioning, the brains were mounted on a freezing microtome (Microm HM430, Thermo Scientific, USA*)* with a 30% sucrose solution. The freezing pad held a temperature of -30°C to ensure that the brains were in a frozen condition before sectioning. Crushed dry ice was used in addition, to keep the brains frozen during the session. The brains were cut in 40 µm thick coronal sections and collected in four separate series. One series was immediately mounted on Superfrost Plus microscope slides in a Tris hydrochloride buffer (Tris-HCl)

solution (Gerhard Menzel GmbH, Braunschweig, Germany), while the three others series were put in DMSO and stored at -20°C for later use.

2.1.6 Staining in Cresyl Violet

In order to precisely delineate cytoarchitectonical borders, one series from each brain was stained with Cresyl violet (Sigma-Aldrich, St. Louis, USA). First, the brain sections, mounted on Superfrost Plus microscope slides (Gerhard Menzel GmbH, Braunschweig, Germany), were dehydrated in graded baths of ethanol (see appendix iV) before being cleared for two minutes in xylene. The sections were then rehydrated in graded baths of ethanol, followed by a quick wash in running tap water. They were then stained in a Cresyl Violet solution, for two to six minutes, depending on the age of the solution and the quality of the tissue. Excess color was removed by alternating the sections between short baths in running water and shorts baths in a solution containing 70% ethanol and acetic acid. If the sections were lightly stained the procedure was repeated until the color and contrast of the sections were sufficiently dark. Finally, the slides were further dehydrated in alcohol and cleared in xylene, before they were coverslipped with a mixture of xylene and entellan.

2.1.7 Image acquistion

Scanner images

All sections used for analysis were scanned with a digital slide scanner using fluorescence illumination (Carl Zeiss, Jena, Germany, model Mirax Midi BF/FL v 1.12) in order to get overview images of the experiments. The scanner was fitted with an Axiocam digital camera (Carl Zeiss, Jena, Germany) and the filter sets 38 (BP 470/40), 43 (BP 545/25) and 50 (BP 640/30) were used to obtain images of cells labelled with different fluorophores from the expression of viral “payloads” and IHC staining.

Confocal microscopy

A Zeiss Meta 510 confocal microscope (Zeiss Imager. Z1, Jena, Germany), equipped with Plan-Apochromat 10x/0.45 NA air, 20x/0.8 NA air and 40x/1.3 NA Oil DIC objectives, was used to capture high quality images of areas containing cells with fluorescent labelling. Different lasers were used to excite different fluorophores. GFP and AF488 were excited by a 488 laser line of an argon laser (dichroic mirror 488nm, emission BP filter 505-550nm), and AF546 was excited using a helium-neon laser (dichroic mirror 561nm, emission BP filter 575-615IR). To get an overview of the fluorescent expression, all sections were first scanned with either a 10x or a 20x objective. When the target area was located, the area of interest was scanned with a 40x oil (NA 1.3) objective in Z-stacks.

Images for delineations

Sections stained with a Cresyl Violet staining technique were used to delineate the borders of brain areas of interest. To obtain pictures of the Cresyl Violet stained sections, images were taken with a camera (CX9000, MBF Bioscience, MicroBrightfield Inc.) mounted on a light microscope (Axio Imager M2, Carl Zeiss, Jena, Germany) through a 5x objective. The images were then imported in Adobe Illustrator CS 6 (Adobe System Inc.) and borders were determined based on cytoarchitectonics and by use of a sterotactical atlas.

2.2 Determining the specificity of the Ssttm2.1 (cre)Zjh/J mouse-line and the distribution of somatostatin cells in the entorhinal cortex

2.2.1 Viral Tracers

A Cre-dependent reporter virus (AAV9-CAG-FLEX-GFP) was injected into the LEC of a SOM-Cre transgenic animal. 1 µL of virus was injected over a time course of 15 minutes. After the injection was completed the needle was kept at the injection site for 10 minutes in order to ensure minimal spread of virus into surrounding brain areas. A more detailed description of the surgical procedure can be found in section 2.1.3 and appendix II.

2.2.2 Immunohistochemistry

An immunohistochemistry (IHC) protocol against the neuropeptide SOM was conducted in order to reveal the SOM expressing cell population in the tissue. The sections were initially washed 3 x 15 min in 0,125M phosphate buffer (PB). The antigen was then unmasked by heating PB to 60°C and letting the sections sit in the heated solution for two hours. The next step involved permeabilization of the sections by washing them2 x 10 min in PB + 1% Triton X (PBT). Afterwards, the sections were pre-incubated for three hours in a blocking solution containing PBT and 10% donkey serum, before they were incubated for 48 hours in an incubation mix containing PBT, 10% donkey serum and 1:400 SOM primary antibody (Goat polyclonal α-SST, Santa Cruz Biotechnology). After the incubation, the sections were washed 4 x 15 min in PB at room temperature (RT) before they were incubated with secondary antibody for 24 hours at 4°C. The incubation mix contained PBT and 1:400 AF546 secondary antibody (IgG donkey α-goat AF546, Invitrogen). The sections were then washed in PB for 3x15 min and mounted on Superfrost Plus microscope slides (Gerhard Menzel GmbH, Braunschweig, Germany) from a Tris-HCL solution. The sections were then air dried overnight on a heating plate set to 37°C and then ultimately coverslipped with a mixture of toluene and entellan. A full list of the IHC protocols can be seen in appendix III.

2.2.3 Counting cells somatostatin immunoreactive cells

In order to count SOM immunopositive somata for analyzing the distribution of SOM cells in the LEC, and for determining the specificity of the mouse line, images from the confocal microscope were used. Z-stacks through the entire thickness using a 40x (NA 1.3) oil objective were made.

For the SOM cell distribution analysis, we delineated horizontal sections from a Cresyl Violet stained series from a brain to identify the LEC, and matched the Cresyl Violet sections with a corresponding series from the same brain, stained against SOM. We then sorted these sections from dorsal to ventral. In total approximately 9 sections that covered the LEC. The most dorsal third of the sections were considered as the dorsal sections, the most ventral third of the sections were considered as the ventral sections, while the last third, in between the dorsal and ventral sections, were considered as intermediate sections of the LEC. We

then selected an area of the LEC, containing a representative amount of cells stained against SOM, from each of the dorsal, intermediate and ventral sections for use in our distribution analysis. The cells within the LEC delineation were then counted and charts showing the distribution were made in Microsoft Excel.

For the mouse line specificity analysis I acquired images from the confocal microscope of all sections that expressed GFP. As I was not able to picture the entire GFP labeled population in each section, I decided to select representative areas from each section. The images were edited with the Zen 2 (blue edition, Zeiss) software before being exported to Adobe Illustrator CS6 for cell counting. The cells were quantified with the help of Microsoft Excel. For normalizing the cell counts to the size of each layers surface area, I used the 'area tool' found in the software Adobe Acrobate XI Pro. As the surface area was measured in pixels and not reflect the actual area of each layer, the normalized cell counts only reflect a relative difference in cell density between each layer.

2.3 Monosynaptic tracing

2.3.1 Viral tracers and injections

For the monosynaptic tracing experiments a total of four different virus strategies were used. All experiments involved injections of two different virus types; An AAV helper virus and a pseudotyped G-deleted RABV. The coordinates used for the injections are described in paragraph 2.1.3. Figure 3 shows a schematic figure that explains the overall concept of monosynaptic tracing.

The first strategy involved two separate injections with an AAV helper virus, serotype 5, expressing TVA, B19 glycoprotein and Green Fluor Protein (GFP) in Cre-positive cells and a later injection of an EnvA-pseudotyped G-deleted RABV expressing mCherry as a fluorescent marker. First 150-200 nL of the AAV helper virus was injected into LEC, followed by a three week incubation period. After three weeks 500nL of rabies virus was injected into the same target location. One week later the animals were perfused and the tissue collected.

The second strategy involved an AAV, serotype 2/1, expressing TVA, CVS glycoprotein and a HA-tag in Cre-positive cells. The rabies virus used here was similar to the one used in the previous strategy, but it expressed GFP as its fluorescent marker and not mCherry. For this strategy both viruses were mixed in the same injection. The total volume of the injections was 600 nL of mixed virus, ⅖ AAV virus and ⅗ RABV. After eight days the animals were perfused and the tissue was collected.

The third strategy involved the same AAV virus as in strategy two. The RABV used was the same as in strategy one. As in the previous strategy, this strategy also involved mixing the two types of virus. 1 µL of mixed virus, ½ AAV virus and ½ RABV, was injected into LEC. For this strategy, the incubation time was two weeks, and the animals were subsequently perfused and the tissue was collected.

The fourth strategy involved the same AAV virus as that used in strategies two and three. The rabies virus was the same as in strategy two, expressing GFP as its fluorescent marker. This strategy involved two separate injections. 400 nL of AAV virus was injected into the LEC. After a two week incubation period 500 nL of RABV was injected into the same coordinate. One week later the animals were perfused and the tissue was collected.

Table 1: Summary of the viral strategies used for monosynaptic tracing experiments.

	Strategy 1	Strategy 2	Strategy 3	Strategy 4
AAV virus	AAV5-synP-FLEX-splitTVA-GFP-B19G	AAV1/2-synP-FLEX-splitTVA-2HA-Gcvs	AAV1/2-synP-FLEX-splitTVA-2HA-Gcvs	AAV1/2-synP-FLEX-splitTVA-2HA-Gcvs
RABV virus	EnvA-pseudotyped, G-deleted rabies mCherry (SADΔG-mCherry)	EnvA-pseudotyped, G-deleted rabies GFP (SADΔG-GFP)	EnvA-pseudotyped, G-deleted rabies mCherry (SADΔG-mCherry)	EnvA-pseudotyped, G-deleted rabies GFP (SADΔG-GFP)
Separate injection	x			x
Mixed injection		x	x	
AAV volume	250-300 nL	240 nL	500 nL	400 nL
RABV volume	500 nL	360 nL	500 nL	500 nL
Incubation time AAV	3 weeks	-	-	2 weeks
Incubation time RABV	1 week	-	-	1 week
Total incubation time	4 weeks	8 days	2 weeks	3 weeks

2.3.2 Immunohistochemistry

In order to enhance the viral expression from the injections, IHC staining was conducted against GFP, mCherry and the HA-tag.

Immunohistochemistry protocol for Green Fluorescent Protein and mCherry

The GFP and mCherry expression from the viruses was enhanced through the same IHC protocol. The tissue was washed in PB for 4 x 15 minutes at RT, before the tissue was permeabilized for 2 x 10 minutes in PBT at RT. After this the tissue was pre-incubated for one hour at RT in PBT containing 5% Natural Goat Serum (NGS). Subsequently, the tissue was incubated for 48 hours in an incubation solution containing PBT, 5% NGS and primary antibodies against both GFP (1:500, IgG rabbit anti-GFP, Life Technologies) and mCherry (1:500, IgG mouse anti-mCherry, Clon Tech). The tissue was then washed for 4 x 15 minutes in PB before it was incubated with secondary antibodies conjugated to florescent markers AlexaFluor488 (1:500, IgG α-rabbit AF488, Invitrogen animal) for GFP, and AlexaFluor546 (1:500, IgG α-mouse AF546, Invitrogen animal) for mCherry. After 24 hours, the tissue was washed 4 x 15 minutes in PB and mounted from a Tris-HCl on Superfrost Plus microscope slides (Gerhard Menzel GmbH, Braunschweig, Germany). When the tissue had air dried on a heating plate overnight, the microscope slides were coverslipped with a mixture of toluene and entellan. A full list of the IHC protocols can be seen in appendix III.

Immunohistochemistry protocol for human influenza hemagglutinin tag

Another IHC protocol was used to visualize the viral human influenza hemagglutinin (HA) tag. First, the tissue was washed in PB at RT for 3 x 15 minutes. Then, in order to enhance permeabilization, the tissue was washed in a solution containing PBT for 2 x 10 minutes. After the permeabilization the tissue was pre-incubated in PBT and 5% NGS for one hour. The tissue was then incubated for 48 hours in PBT, 5% NGS and a primary antibody against the HA-tag *(1:200 primary antibody)* at 4°C. After 48 hours the tissue was washed 4 x 15 minutes in PB, before it was incubated for 24 hours with a secondary antibody. The incubation mix contained PBT and goat anti-rat AlexaFluor 633 (1:400, IgG goat α-rat AF633,

Invitrogen) and was kept at 4°C in a refrigerator. The following day, the sections were washed 4 x 15 minutes in PB and mounted on Superfrost Plus microscope slides (Gerhard Menzel GmbH, Braunschweig, Germany) in a Tris-HCL solution. The sections were then air dried on a heating plate overnight, before they were coverslipped with a mixture of toluene and entellan. A full list of the IHC protocols can be seen in appendix III.

2.3.3 Counting cells for monosynaptic tracing

Neurolucida

In order to trace cells expressing fluorescent markers we used the computer program Neurolucida (MBF Bioscience, MicroBrightfield Inc.), coupled to an Axiomager M2 microscope (Carl Zeiss, Jena, Germany). The contour of each brain section was outlined using the "contour" tool in Neurolucida using a Plan-Apochromat 2.5x/0.0075 NA air objective. For the cell counting, I used a Plan-Apochromat 20x/0.8 NA air objective and the "meander scan" tool in Neurolucida to ensure that the entire section was analyzed. Filters reflecting light at different wavelengths were used to reveal the fluorophores AF488 (emission BP filter 505-550nm) and AF546, GFP and mCherry (emission LP filter 655nm) in the tissue.

The counts of monosynaptic labelled cells were performed with the help of an Axiomager M2 microscope and the software Neurolucida. The section was inserted in to the microscope and the contour of each sections were outline with the help of the "contour" tool found in Neurolucida. To ensure that the entire section was scanned, I used the "Meander Scan" tool. For each time I scanned a new part of the section, I switched between two different filters to check for cells expressing the two different fluorescent markers I applied to AAV and RABV viruses. I used two different software labels in Neurolucida to mark and distinguish starter cells and monosynaptically connected cells. When all the sections had been processed, I imported the contours and the labels to Adobe Illustrator, where they were matched with a corresponding Cresyl Violet stained section. The labels were used as representations of cells, The areas that expressed cells were delineated and the cells within each area was quantified.

2.4 Delination

Delineations of different brain regions were done by looking at Cresyl Violet stained brain sections cut in the coronal plane. Both the Paxinos stereotactical atlas (Franklin K. B. J., 2007) and cytoarchitectonic features previously defined in the literature were used in order to characterize and describe the cytoarchitectonic borders between brain regions. Only brain areas that expressed a significant number of GFP cells in the monosynaptic tracing experiment are described in this section, areas expressing only minute numbers of cells are not characterized here.

2.4.1 Delineation of the lateral entorhinal cortex

The EC is a six-layered cortex, usually divided into a lateral and medial domain (the LEC and the MEC respectively) (Boccara et al., 2015). When delineating the LEC for this project, it was considered as one entity, even though it has previously been subdivided into smaller structures (Insausti et al., 1997, Cappaert et al., 2015). LI of the LEC is a rather narrow layer and can easily be identified on the basis of its relatively cell free appearance. In some parts of the LEC however, LI can contain a few cells that look like displaced layer II cells (Insausti et al., 1997). The border between LI and LII is distinguished with a sudden increase in cell size and cell density. The transition between LII of MEC and LEC was identified on the base of the relatively smaller cell size and more scattered distribution of cells in LII of the LEC, which is a feature supported by other studies (Boccara et al., 2015). Cells in LII also tends not to form a continuous layer, but instead cluster into islands of cells. As LIII contains smaller cells than LII and is not that densely packed (Cappaert et al., 2015), I identified the transition between LII and LIII on the base of a decrease in cell size and density. In our sections, layer IV was not conspicuous, which stands in clear contrast with the sharp lamina dissecans seen in the MEC. Even though layer IV didn't present any major separation between layer III and V, the two layers can be easily distinguished since layer V contains larger cells, which are described as big and dark pyramidal cells by Insausti (Insausti et al., 1997). The deep layers, respectively layer V and VI, lack a clear columnar organization and the two layers are hard to separate from each other, even though layer VI is described to be more compact than layer V (Boccara et al., 2015). As the border between LV and LVI is hard to distinguish in Cresyl Violet

sections these two layers were not separated in our thesis. The different layers of the LEC were delineated and then categorized into superficial (LI,II,III) and deep (LIV,V,VI) layers. For our distribution analysis I also delineated the LEC in horizontal sections, and the borders were established on the same criteria that was presented here. A figure of a delineated area of the LEC in a coronal section can be seen in figure 6.

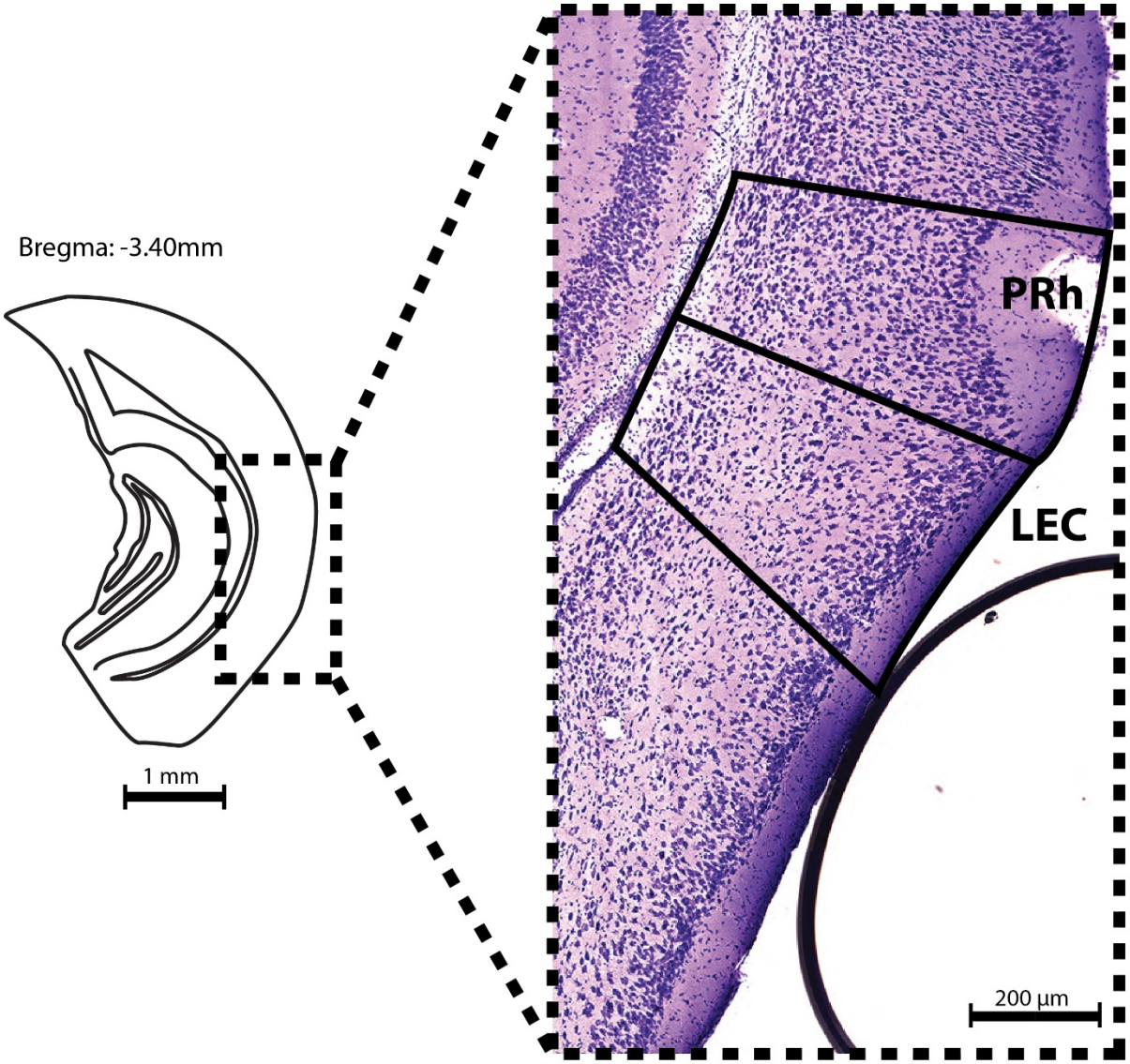

Figure 6: Delineated Cresyl Violet stained section of the LEC and the PRh. The figure shows the LEC and the PRh with its medial, dorsal and ventral borders, illustrated by black lines. The cartoon on the left illustrates the position of the picture within a coronal section of the mouse brain.

2.4.2 Delineation of the piriform cortex

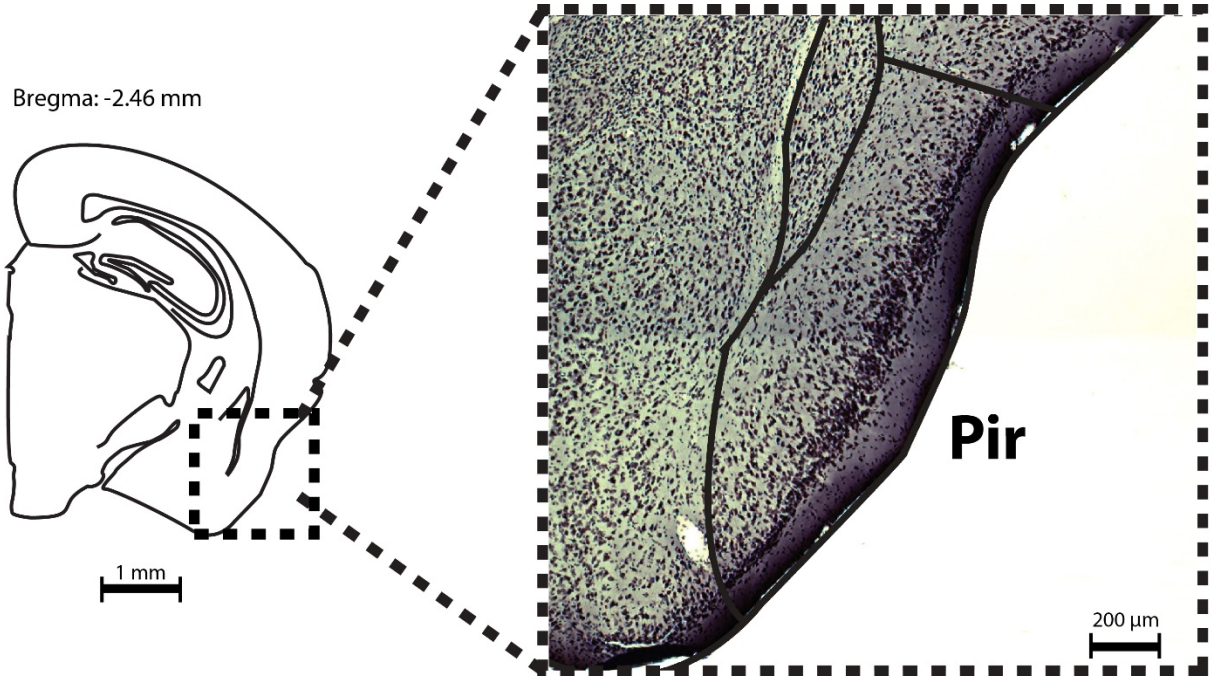

Figure 7: Delineated Cresyl Violet stained section of the Pir: The figure shows the Piriform cortex, and the black lines indicate the borders of the Pir. The cartoon on the left illustrates the position of the picture within a coronal section of the mouse brain.

The Pir (Figure 7) is a three layered cortical structure which is located ventral to the rhinal sulcus (Vaughan and Jackson, 2014). The Pir borders the anterior olfactory nucleus rostrally, the LEC and amygdala caudally, and dorsally it is borders by the insular and perirhinal cortices. The medial border of the Pir is to several subcortical nuclei. I identified the Pir by a cell sparse LI followed by a densely packed LII with darkly stained principal neurons, and LIII had more loosely arranged pyramidal cells (Suzuki and Bekkers, 2006). Borders of the Pir to the LEC and PRH could easily be identified as the latter two are six layered structures, and the transition from three to six layers could be seen clearly. The border to the insular cortex could be found by looking at the arrangement of LII cells which is denser in the Pir compared to the insular cortex. Anteriorly, our cell labelling did not extend towards the border to the anterior olfactory nucleus, hence this border is not described here. Borders to subcortical structures could be identified by their lack of lamination.

2.4.3 Delineation of the perirhinal cortex

The PRh is situated around the rhinal sulcus of the rodent brain, and although the PRh can be subdivided into two substructures, areas 35 and 36 (Boccara et al., 2015). I have not used these subdivisions in our analysis. The features used to separate the PRh from surrounding areas are a lack of cellular distinction between LII and III (Cappaert et al., 2015) and poorly developed LIV. I also saw that the cells in LII of the PRh were generally smaller and not as darkly stained as in the surrounding areas. Rostrally the PRh borders the insular cortex, caudally it borders the postrhinal cortex, dorsally the temporal association area and the postrhinal cortex, and the ventral border is with the LEC. This ventral border was clearly visible when investigating cytoarchitectonic features. The superficial layers of the LEC showed a clear lamination, while similar layers in the PRh did not (Boccara et al., 2015). The border beween the insular cortex and the PRh was recognized based on the architecture of LV, as the PRh cells looked more elongated compared to those in the deep layers of the insular cortex. LV in the PRh was also thicker than LV in the insular cortex. Additionally, LV and IV of the insular cortex are known to be approximatley of equal thickness, while LV of PRh was found to be substantially thicker than LIV (Burwell, 2001). A delinated area of the Prh can be seen in figure 6.

2.4.4 Delineation of the hippocampus

The CA field of the hippocampus is divided into three subfields, the CA1, the CA2 and the CA3 (Figure 8). The laminar organization for these three fields is generally the same. The most prominent layer where the principal neurons are found is called the pyramidal layer, or stratum pyramidale. Deep to this layer lies a relatively cell-free layer called the stratum oriens. Superficially to the pyramidal layer lies the stratum radiatum, while most superficially the stratum laconosum moleculare is situated. A feature of the CA3, which is not found in the CA1 or the CA2, is the stratum lucidum, which is a narrow cell free layer with a light appearance, located just above the pyramidal layer. The end of stratum lucidum marks the border between CA3 and CA2 (Gulyas and Freund, 1996, Boccara et al., 2015, Cappaert et al., 2015).

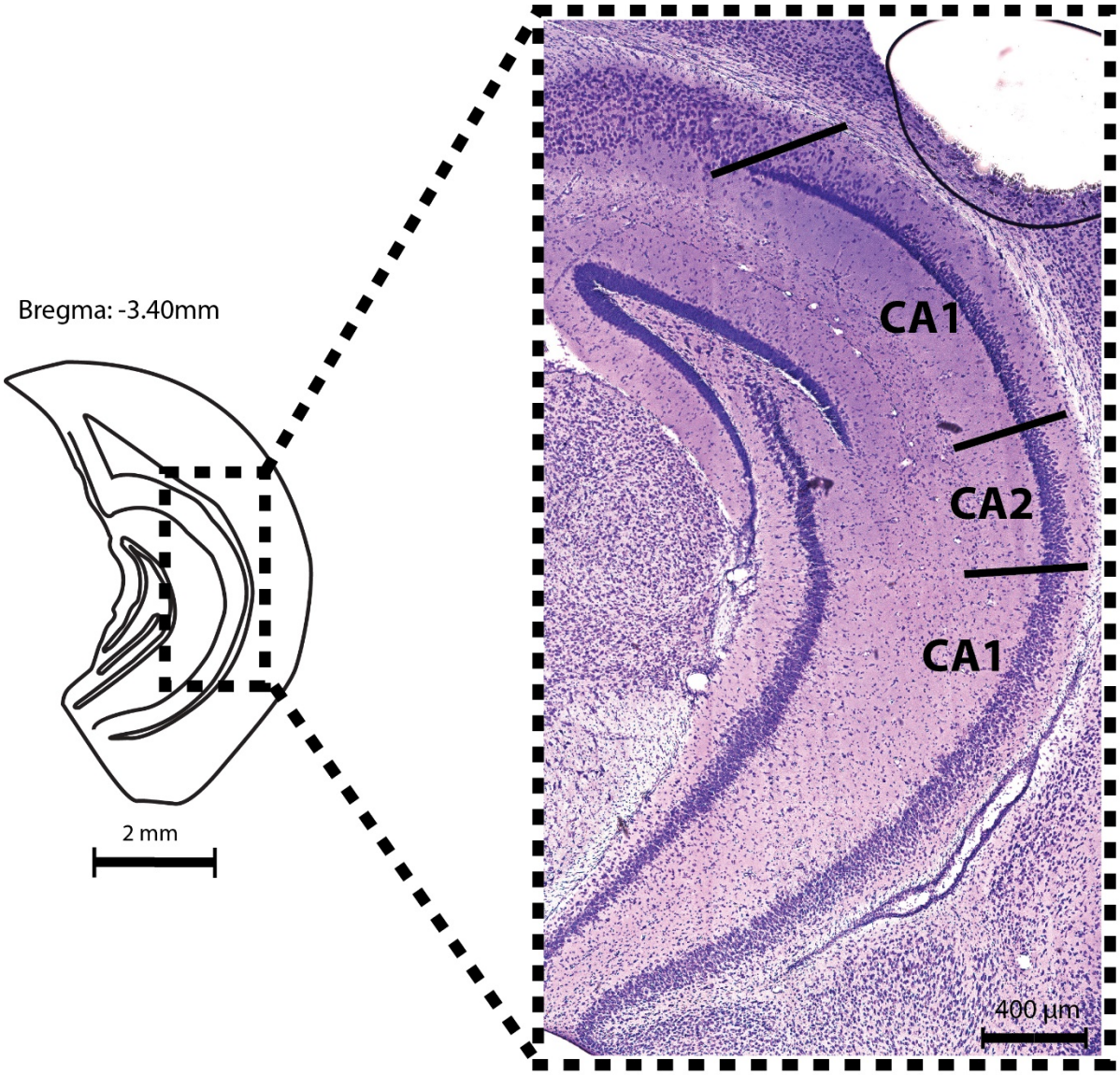

Figure 8: Delineated Cresyl Violet stained section of the CA1 and CA2. The figure shows the CA1 and the CA2 illustrated by the black lines. The cartoon on the left illustrates the position of the section within a coronal section of the mouse brain.

Cornu Ammonis 1

The CA1 borders the Sub at its most distal end part the CA2 proximally (Boccara et al., 2015). The CA2 contains a mixture of large and small pyramidal cells, thus the border between the CA1 and the CA2 could be distinguished by a pronounced increase in pyramidal cell size at the proximal CA1 border (Cappaert et al., 2015). A sudden widening of the pyramidal cell

layer, together with less darkly stained pyramidal cells, characterized the border between the CA1 and the Sub (Boccara et al., 2015).

Cornu Ammonis 2

The stratum pyramidale in the CA2 contains large and darkly stained pyramidal neurons and borders the CA1 distally and the CA3 proximally (Cappaert et al., 2015). Large and small pyramidal cells are mixed together in the CA2, and this can be used to characterize its borders. The large pyramidal cells are similar to those reported in the CA3, while the smaller pyramidal cells looks like the cells seen in the CA1 (Boccara et al., 2015).

3. Results

3.1 Specificity of the Ssttm2.1(cre)Zjh/J mouse line

The specificity of the transgene expression in our mouse line was checked in two animals. This part of the project was a collaboration with another master's student in the lab, Martin Øvsthus. An AAV viral vector, which expressed GFP in the presence of Cre recombinase, was injected into our area of interest. I carried out an IHC protocol against SOM in order to reveal the SOM expressing cell population in the tissue.

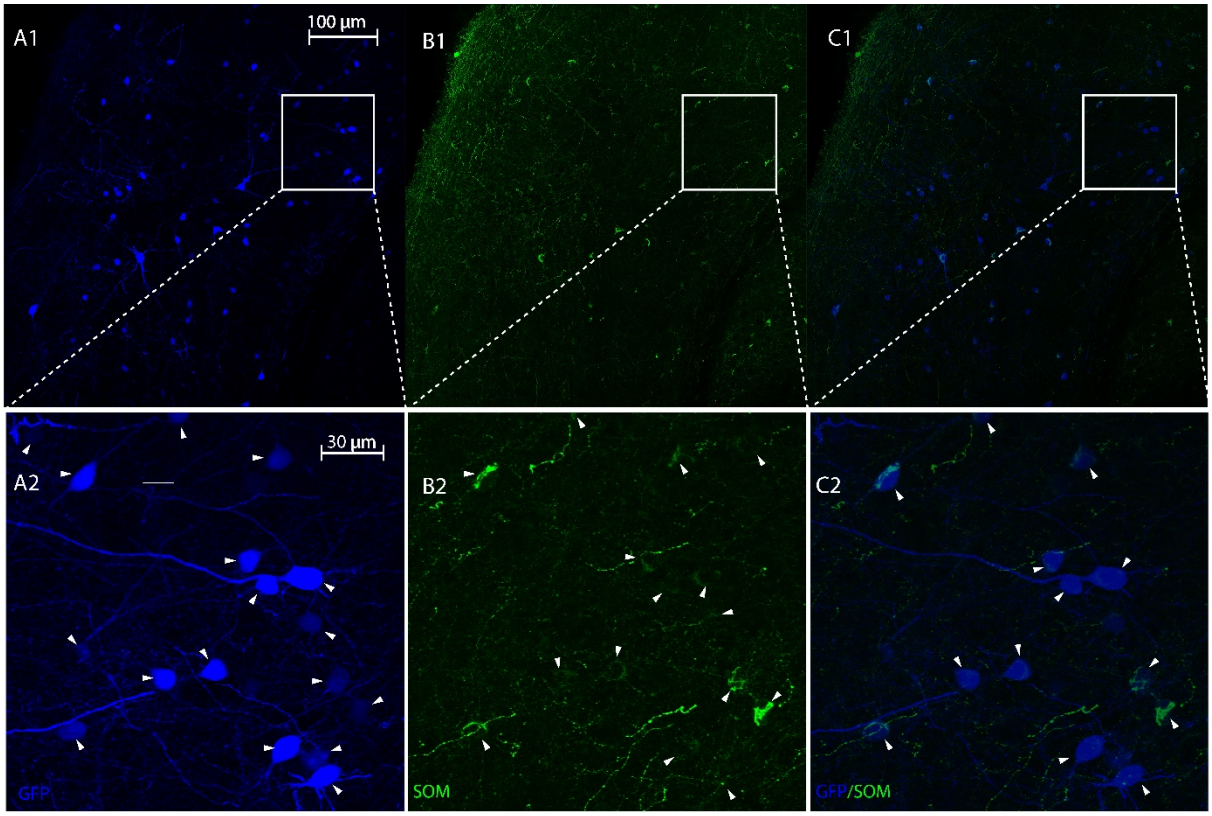

Figure 9. Image of the GFP expression and immunostaining against SOM. (A1) Overview of cells expressing GFP. **(A2)** Close up picture of cells expressing GFP. White arrows indicate GFP positive cells. **(B1)** Overview of cells labelled for SOM. **(B2)** Close up picture of cells labelled for SOM. White arrows indicate SOM positive cells. **(C1)** Overview picture of overlapping GFP and SOM populations. **(C2)** Close up picture of overlapping GFP and SOM populations. White arrows indicate double labelled cells.

Overlap between the GFP and SOM IHC was counted in order to analyze the specificity of the transgene expression in the mouse line. As regular fluorescence microscopy did not identify immunopositive cells reliably, I used images taken with the confocal microscope to perform the cell counts. Figure 9 shows confocal pictures of cells labeled with GFP (A1 and A2), SOM (B1 and B2) and an overlay of the two stains (C1 and C2). In both cases the transgene expression had a high specificity (82 and 84% overlap with SOM IHC), and I did not see any differences related to the specificity across the dorsoventral axis (data not shown). Figure 10 shows the total population of cells labeled with GFP (red) and the percentage of cells labelled with both GFP and immunohistochemistry against SOM (blue) in the two animals. The third histogram shows the average between the two cases, which was found to be 83%.

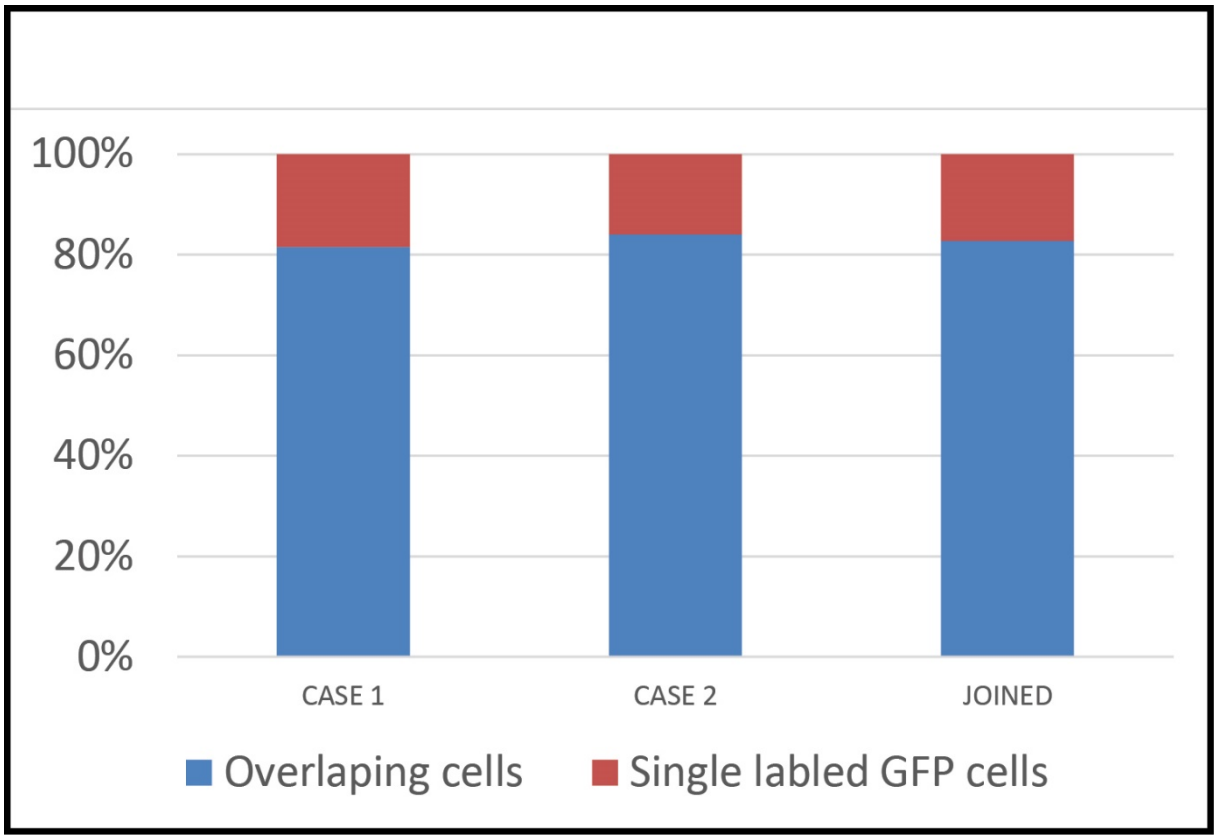

Figure 10. **Overlap between transgene expression and immunohistochemistry against somatostatin.** Chart showing the amount of GFP positive cells (red) and the amount of GFP cells which overlapped with the SOM population (blue) in two different cases. The joined graph show the combined results of case 1 (n=411/504) and case 2 (n=173/206).

3.2 Distribution of SOM positive cells in the lateral entorhinal cortex

The analysis of the distribution of SOM cells in the LEC was performed in one of the animals that had been used to characterize the mouse line (case 1). The distribution of SOM cells was described based on IHC data from in horizontal sections of the mouse brain. Three slices were selected to represent respectively the dorsal, intermediate and ventral portions of the LEC, and the area was delineated using Cresyl Violet stained sections from the same animal. Figure 11 shows the three different sections of the LEC that were used for the count (A1, B1 and C1), with corresponding confocal images from the counting areas (A2, B2 and C2) as well as schematic figures of the cell counts (A3, B3 and C3).

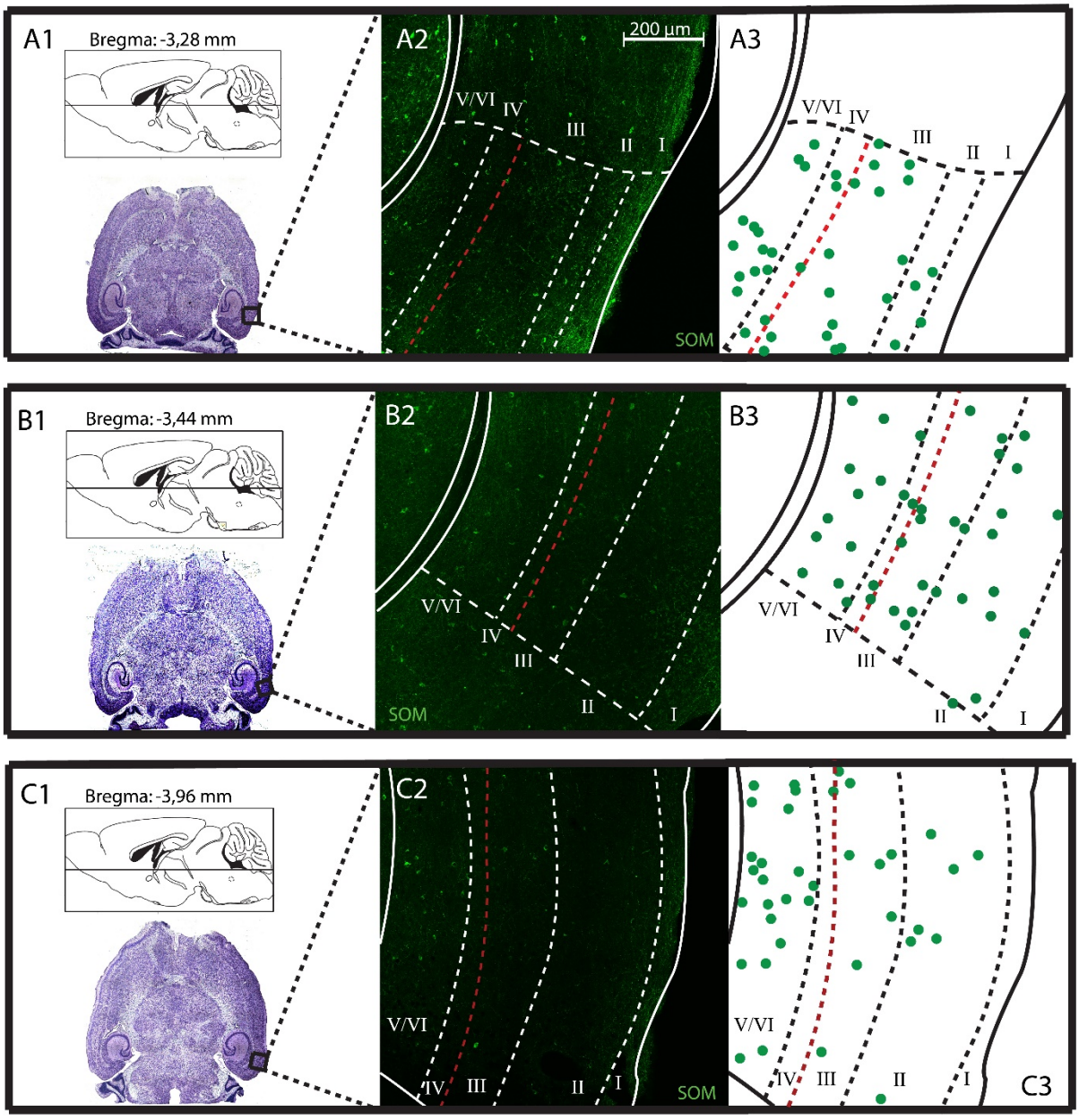

Figure 11: Areas of the lateral entorhinal cortex used to map the distribution of somatostatin cells: (A1-B1-C1) Horizontal sections of the mouse brain displaying the dorsal, intermediate and ventral sections of the LEC, used for the distribution analysis. The black square indicates the outer border of the confocal image seen in A2-B2-C2. **(A2-B2-C2)** Confocal images used for counting SOM positive cells within the LEC. The LEC was delineated using the Cresyl Violet stained section in A1-B1-C1. The red dashed line indicates transition between superficial and deep layers. **(A3-B3-C3)** Shows the cells (green dots) counted within the LEC. The schematic drawings of the midsaggital view of mouse brain (seen in A1-B1-C1) is adapted from Franklin and Paxinos (2007)

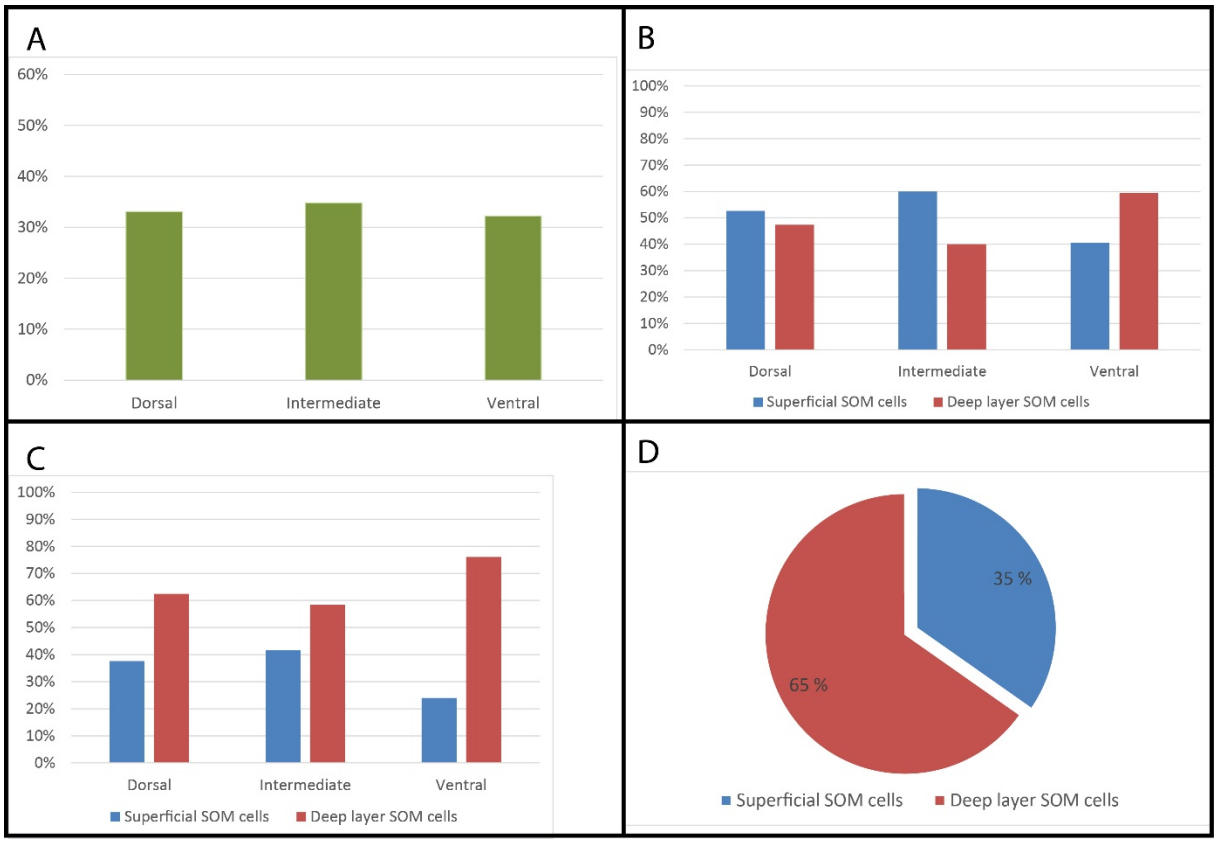

Figure 12: Distribution of somatostatin cells in the lateral entorhinal cortex. (A) The cell counts in dorsal (n=38), intermediate (n=40) and ventral parts (n=37) of the LEC, showed in percentage of the total cell count within the LEC. **(B)** The cell counts in superficial and deep layers of dorsal, intermediate and ventral sections of the LEC, showed in percentage of the total cell count within the respective section. **(C)** The cell density in superficial and deep layers of dorsal, intermediate and ventral sections of the LEC, showed in percentage of average cell density within the respective section **(D)** Pie chart showing the difference in cell density between superficial and deep layers of LEC as a whole.

The total number of SOM positive cells in the LEC along the the dorso-ventral axis was found to be very consistent and each section in the dorso-ventral axis contained approximately one-third of the total number of counted SOM positive neurons (figure 12 A). Considering the layer distribution throughout the dorso-ventral axis, it appeared that there was a laminar preference towards superficial layers in ventral and intermediate sections, while it was reversed in the most dorsal section (Figure 12 B). However, as the different layers vary in size, I normalized the cell counts to the size of the surface area of each layer which made it

clear that the cell density was highest in deep layers of the LEC for all of the three sections (Figure 12 C). When considering distribution across layers in the LEC as a whole, I found clear indications that most SOM cells were situated in deep layers of the LEC (65%), compared to the superficial layers (figure 12 D).

3.3 Viral strategies

Four different strategies for the monosynaptic tracing experiments were employed. The strategies were tested in collaboration with another master's student at the lab, Martin Øvsthus. Strategy 1 resulted in one case of good viral transport, one case of poor viral transport and two cases of no viral transport.

Table 2: Outcome of the different viral strategies used for the monosynaptic tracing experiments. The table shows the number of cases that expressed either good viral transport, poor viral transport or no viral transport for the different viral strategies I used for our MEC and LEC injections. The numbers flanked by parentheses show the number of injections that missed the targeted area. The * indicates a case of anterograde transport

	Cases of good viral transport		Cases of poor viral transport		Cases of no viral transport	
	LEC	MEC	LEC	MEC	LEC	MEC
Strategy 1	0	1	1	0	1	1
Strategy 2	0	0	0	1	1	2
Strategy 3	2 - (2)	0	1	1	1	2 – (1)
Strategy 4	2 - (1)	0	0	1*	0	0

Strategy 2 had no viral transport for the LEC experiments, while one brain expressed sparse local transport in the MEC. Strategy 3 had two experiments expressing a good viral transport, however both injections were slightly misplaced. Two brains expressed only local transport, while three cases were not successful. Strategy 4 had two cases in the LEC experiments which both had good viral expression, however in one of the cases the injection

site were misplaced. The case for the MEC experiments expressed an unusual expression where it looked like the virus had been transported anterograde. A complete list of the outcomes of the different tracing strategies can be seen in table 2.

3.4 Monosynaptic inputs to somatostatin inteneurons in the lateral entorhinal cortex

Monosynaptic inputs to SOM INs were traced using the viral approach described earlier in the thesis, the results shown here are from a single animal injected with the forth injection strategy described. Due to difficulties with the immunohistochemistry against the HA tag carried by the helper virus, I were not able to characterize the starter population to which the monosynaptic inputs were traced or whether this was entirely confined to the LEC. All sections from our monosynaptic tracing experiment were cut in the coronal plane. As I were unable to characterize the starter population, it is difficult to position the exact location of the injections site. However, due to the viral expression I assume that the injection site is situated close to the dorsal border of the LEC

3.4.1 Monosynaptic inputs from the parahippocampus and pirifrom cortex

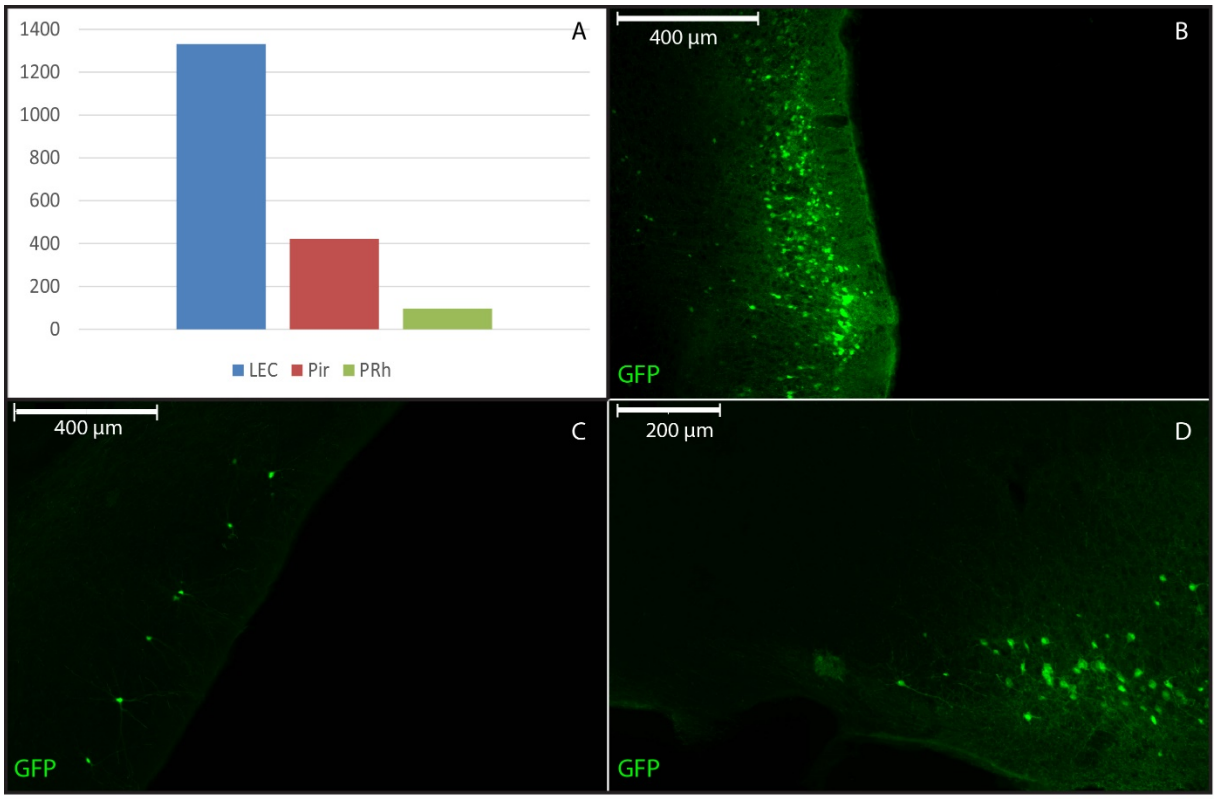

Figure 13: Monosynaptic inputs to the LEC SOM cells from the LEC, the Pir and the PRh. **A:** A chart showing the total number of cells counted within each brain area in the monosynaptic tracing experiment. **B:** Overview picture of rabies labeled cells in the LEC **C:** Overview picture of rabies labeled cells in the Pir **D:** Overview picture of rabies labeled cells in the PRh. Pictures in B, C and D are taken with a Mirax Scanner. For the full names of the different brain areas, look in the abbreviation list at page xi.

The highest density of monosynaptic inputs to SOM cells in the LEC was detected within the LEC itself and in brain areas close to the LEC, particularly in the PRh and the Pir. Figure 13 A shows cell counts and overview pictures of counted cells in these areas.

The overall highest cell count was made in the LEC (1331 cells). The GFP expressing cells within this area were mostly confined to the superficial layers where they were rather densely packed together. The highest density of rabies cells were found in LII, some cells were found in LIII, while LI was almost free of traced cells (Figure 13 B). A small portion of traced cells were also found in deeper layers. Close to the injection site, which was located ventrally in the LEC, the highest density of cells was found close to the border with the Pir.

However, in more posterior sections, further away from the injection site, the GFP expressing cells in the LEC were more evenly distributed across the dorsoventral axis with no clear preference for either region.

A substantial number of GFP expressing cells were found in the Pir (421 cells). Even though there were several exceptions, it seemed that most monosynaptic inputs from the Pir originated in LII. Figure 13 C is a picture of an anterior portion of the Pir, where all rabies cells are located within LII. In anterior sections of the brain the GFP rabies labelling was scattered with no clear preference for either dorsal or ventral parts. However, in more posterior sections when the Pir starts to border the LEC dorsally, the GFP expression was more confined to the area close to the dorsal border of the Pir. Close to the injection site, the rabies cells in the Pir seemed to form part of the same cluster of GFP expressing cells that was seen in ventral parts of the LEC, due to this I suspect that starter cells may also be present in the Pir.

Although the cell counts were smaller compared to the LEC and the Pir, a fair amount of rabies cells (96) were counted within the PRh. The distribution of rabies cells in the PRh was strikingly similar to the superficial and deep layer distribution seen in the LEC, most cells in the PRh were seen in superficial layers with the highest density in LII and III, and with fewer rabies cells located in deeper layers. . The highest density of PRh cells was seen close to the ventral border to the LEC in the most posterior sections of the brain. Other regions of the PRh had more sparse representations of cells. An image of the rabies expression in the PRh can be seen in figure 13 D.

3.4.2 Monosynaptic inputs from the hippocampal Formation

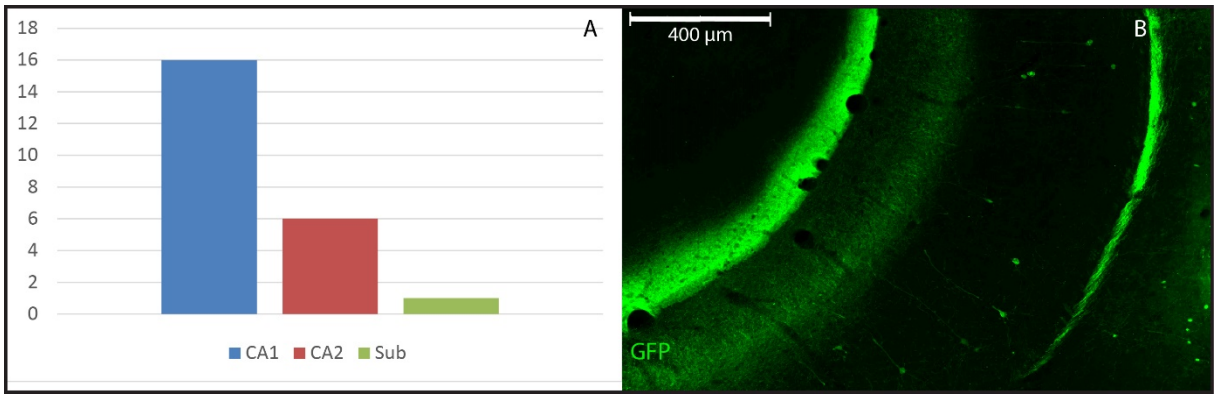

Figure 14: Monosynaptic inputs to SOM cells in the LEC, from the Hippocampal formation. A: Total number of cells counted within the CA1, the CA2 and the Sub. B: Overview picture of rabies cells in the CA1. For the full names of the different brain areas, look in the abbreviation list a page xi.

Cells in the HF also provide inputs to LEC SOM cells. The CA1, the CA2 and the Sub were the three subfields of the HF that contained rabies cells, the cell counts and an overview picture from the HF are shown in figure 14**.** Except for the most anterior sections of the brain, the HF is visible through most sections of the brains. However, cells expressing GFP were only found in the most posterior portions of the HF. The CA1 had the highest number of rabies cells, with a total of 16 cells, most of the cells were found within the stratum pyramidale. However, some cells in the CA1 were located deep to the pyramidal layer, in the stratum oriens. A few cells (6) were located in the CA2, all within the pyramidal layer. One single cell was found in the pyramidal layer of the Sub, right on the border to the CA1.

3.4.3 Monosynaptic inputs from subcortical structures

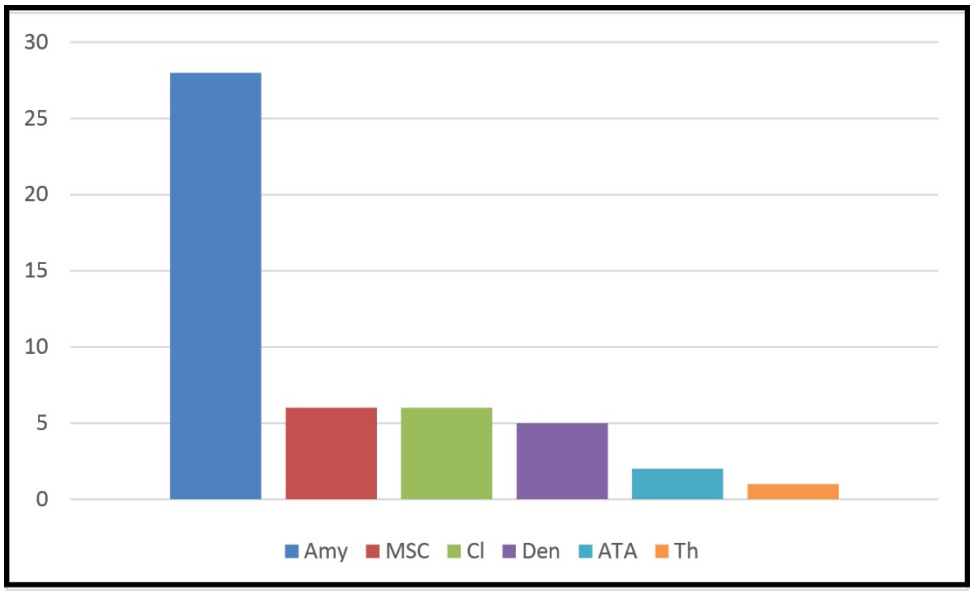

Figure 15: Total number of cells counted in subcortical structures. For the full names of the different brain areas, look in the in the abbreviation list a page xi.

Our experiments showed that the SOM cells in the LEC received inputs from a number of subcortical areas. Figure 15 shows a quantification of cells within different subcortical regions. Input cells originating in the amygdala were the most abundant in the subcortex, 28 cells were counted in different amygdaloid nuclei. For simplicity I have treated the amygdala as one big structure. However, this is a gross oversimplification as the amygdala is a complex structure containing several different substructures with unique properties. The cells found in the amygdala were scattered across the area, indicating that the cells indeed are located in several nuclei. The claustrum, consisting of both the anterior claustrum (Cl) and the dorsal endopiriform nucleus (DEn) also innervated the SOM IN population in the LEC relatively strongly compared to other subcortical structures. Six cells in the Cl were found distributed throughout the anteroposterior axis of the structure, with no particular preference for either anterior or posterior portions of the brain.

Six rabies infected cells were found in the medial septal complex, which consists of the medial septal nucleus (MS) and the nucleus of the diagonal band with a horizontal and a vertical limb (HDB and VDB nucleus respectively). After delineation one cell was classified as

being situated in the HDB nucleus. In the VDB nucleus a total of three cells was found. The two last cells were found in the MS. The most anterior cell was situated in ventral parts of the section, close to the nucleus of the diagonal band. The second cell found in the MS was situated more dorsally and close to the midline of the brain. The cells in the medial septal complex were never clustered together. Single cells giving inputs to SOM cells in the LEC were also located in the thalamus and the amygdaloidstriatal transition area (ATA).

3.4.4 Monosynaptic inputs from other cortical areas

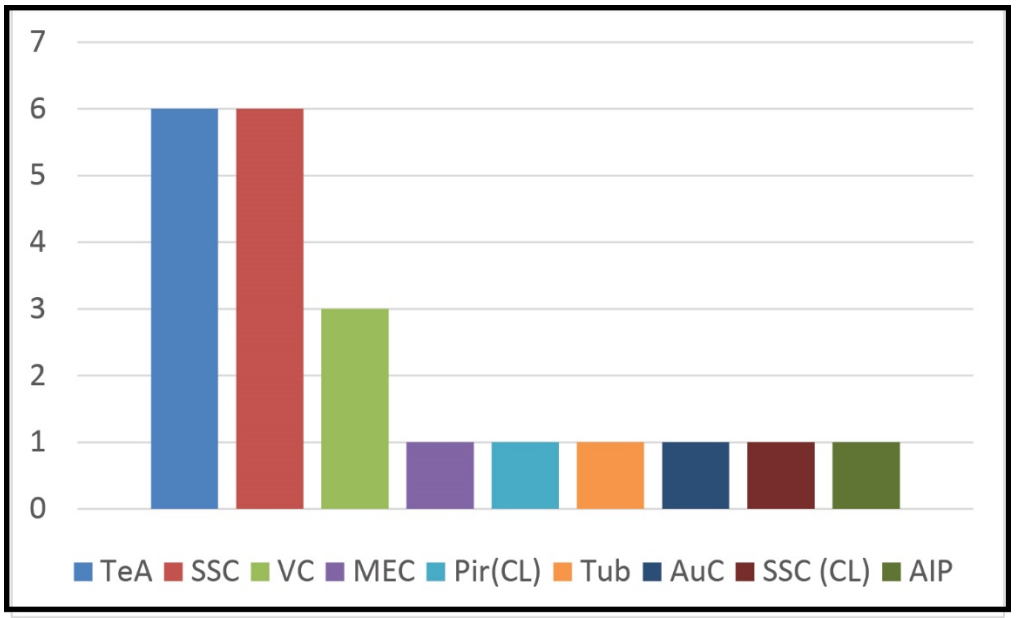

Figure 16: Total number of cells counted in other cortical areas. For the full names of the different brain areas, look in the in the abbreviation list at page xi.

Sparse expression of GFP in single cells was observed in different cortical areas, other than the ones previously described. Figure 16 shows a quantification of inputs from different cortical areas. The temporal association cortex had a total of six rabies infected cells, all of these cells were found in the same section, in the posterior extreme of the brain. Six GFP expressing cells were seen in the somatosensory cortex, and all of them were located in superficial layers. A single cell was also positioned in the contralateral somatosensory cortex. In posterior portions of the brain three cells expressing GFP were situated in the visual cortex. A single cell was found in the contralateral Pir in an anterior section of the brain. One

cell, found in the MEC, was situated in deeper layers, and one cell in the olfactory tubercle was located in the anterior extreme of the brain, in close proximity to the Pir border. One cell within the auditory cortex was found in intermediate sections of the brain, situated in superficial layers of the cortex. The last cell was found within the insular cortex in an intermediate section of the brain and it was situated in superficial layers of the cortex.

4. Discussion

4.1 Methodological considerations

4.1.1 Somatostatin immunohistochemistry and cell counts

The IHC staining in somata of SOM cells was relatively weak, and we had trouble identifying SOM positive cells using regular fluorescence microscopy. The weak soma labelling observed is due to the low concentration of SOM in cells bodies, as it is only synthesized in the soma and later transported to the axon terminals for release (Mains RE, 1999). Using a regular fluorescence microscope it was difficult to filter out-of-focus light from different levels of the sample. Hence, it was hard to distinguish the weakly labelled somata from the out-of-focus background staining and auto fluorescence. To overcome this obstacle I decided to perform the cell counts using a confocal microscope, as this could give precise optical sections from the sample. A limitation to the use of a confocal microscope for counting cells is that it is very time consuming compared to other counting techniques used in our lab.

4.1.2 Starter cells

The IHC I used for the HA tag in the monosynaptic tracing experiment did not work reliably. Although I were able to produce successful staining in other samples, the stain failed to identify starter cells in our monosynaptic tracing experiment for reasons that are unclear to me. Due to the trouble with the IHC I was not able to identify the exact location of the starter population. However, looking at the density of rabies infected cells around the mechanical damage from the injection needle, I speculate that the majority of the starter cells were situated close to the border of the Pir in the anteroventral portion of the LEC. The input to the SOM cells may thus be biased towards afferents terminating in this distinct topographical area of the LEC. Looking at the density of rabies infected cells in this particular area, I also conclude that it is likely that starter cells were also present in the Pir.

4.1.3 Delineations

The Cresyl Violet technique was in general sufficient for establishing the cytoarchitectonic borders of different areas. However, I experienced some difficulties delineating subcortical complexes containing a set smaller sized nuclei. Even though I relied on both the atlas by Franklin and Paxinos (2007) and the cytoarchitectonic features of our stained sections, establishing accurate borders between the different nuclei proved to be difficult. We thus decided to enclose some subcortical complexes as a whole, and not delineate them any further.

A limitation delineating areas exposed to viral injections, is that the injection causes mechanical damage at the injection site, which in turn forms gliosis in the tissue. As a consequence, delineating the ventral border of the LEC for our monosynaptic tracing experiments was in some sections more difficult, as the gliosis altered the cytoarcithecture of the area. In order to overcome the issue with gliosis I could have used other staining techniques. Such as IHC against the glycoprotein Reelin, which is expressed in cells in layer II of the EC, but not in some of the adjacent areas (Stranahan et al., 2011). Staining for Reelin could thus have been an alternative approach for delineating the borders of the LEC.

4.2 Specificity of the Ssttm 2.1(cre)Zjh mouse line

The overlap between the Cre expressing cells in our transgenic mouse line and the IHC staining against SOM was found to be 83%. This was an average of data two animals, and the variation between the counts in the two animals was minimal. Hence, it seemed that the transgenic mouse line was consistent in its Cre expression across individuals. Even though these results tell us that the mouse line is highly specific for SOM cells, 17% of the Cre-expressing cells were found to be outside the SOM population. As the IHC stain against SOM was weak and only partially labelled the soma, this may have led to some cells not being counted as SOM positive, and that our results reflect and underestimation of the actual overlap percentages. On the other side, there is a possibility that Cre can be expressed in cells that did not undergo recombination due to insertional effects of the transgene, (Lewandoski, 2001, Hu et al., 2013). This way some cells outside the targeted SOM population will express Cre and will lead to an error.

4.3 Distribution of Somatostatin positive cells in the lateral entorhinal cortex

SOM cells were found in all regions and layers of the LEC. No difference in the SOM cell distribution could be seen across the dorsoventral axis. However, across laminae there was seen a clear preference towards deeper layers. Even though results contradicting mine have been reported (Wouterlood and Pothuizen, 2000), most studies support my findings with regards to the distribution pattern of SOM cells both in the EC and in other cortical structures (Kohler and Chan-Palay, 1983, Morrison et al., 1983, Nassar et al., 2015, Phan, 2015, Øvsthus, 2016). The laminar preference seen in my data was maintained throughout the dorsoventral axis, and was even more evident when the data was normalized to the surface area of each layer. The high number of SOM expressing cells in deeper layers contrasts with the distribution of other IN populations in the LEC. The VIP and PV populations have been found throughout all layers, but both have been shown to have a preference for superficial layers of the LEC (Kohler and Chan-Palay, 1983, Wouterlood et al., 1995). My data thus show that SOM INs constitute a large portion of the IN population of deep layers in the LEC, and indicate that other IN groups are likely more common in superficial layers.

The majority of SOM expressing INs in the (neo)cortex have been reported to be MCs (Wang et al., 2004). When I compare my SOM cell data from the LEC with the typical characteristics of MCs there are similarities. MCs are present in all layers of the (neo)cortex, but more abundantly in deeper layers (Wang et al., 2004), just like the SOM positive cells in this study. Additionally, my IHC staining shows a dense plexus of SOM immunoreactive axonal fibers in LI, which is a typical morphological feature of MCs (Wang et al., 2004). Thus, my results indicate that the SOM positive cells in the LEC might belong to the groups of MCs described in the (neo)cortex, although I was not able to fully characterize the morphology.

4.4 Viral strategies

During our monosynaptic tracing experiments we tested four different viral injection strategies in order to optimize the long-distance monosynaptic transport of our rabies virus.

Our first strategy involved two separate injections of AAV and RABV, and used a relatively long incubation period. The injection volume was kept small in order to ensure expression within a confined area. However, with only one case of good viral transport, I speculate that a low volume of virus also leads to fewer viral particles present in the tissue, hence a weaker viral expression. With small volume injections there is also a lower likelihood for the two viruses to infect the same cells which is a requirement for viral transport.

For the second strategy we decided to do an injection of mixed virus. To keep the virus injection confined within a small area of space, we performed a small volume injection. In addition, the incubation period in this strategy was 8 days, which is considered as relatively short. Alongside a low injection volume, we speculate that the poor viral transport could have been a result of a short incubation period, which gave the viruses insufficient time to express their genes. Another possibility is that the virulent nature of the RABV virus affects the general health of the cells, which in turn affects the “payload” expression of the AAV virus (Wickersham et al., 2007, Callaway and Luo, 2015).

Except for an extended incubation period and an increased injection volume, the third strategy was similar to the second strategy. The increased incubation period should ensure the viruses more time to express their “payload”, while an increased volume should lead to a higher amount of virus particles present in the tissue, and thus an increased likelihood for a good viral expression. However, a disadvantage of a large volume seems to be that it is difficult to keep the injection within a confined area (Aschauer et al., 2013). This strategy gave us some cases of good viral transport, however it seemed to be to be an unreliable strategy, as the results varied widely from case to case. I speculate that this unreliability could be due to the virulent nature of the RABV virus, as previously mentioned.

For the last strategy, we went back to two separate injections of virus. As large volume injections had clear disadvantages, we tried to decrease the injection volume a bit. Separate injections, with a long incubation period and an intermediate amount of virus should increase the likelihood of obtaining a good viral expression, but the risk is still that the virus possibly could leak out of the targeted area (Aschauer et al., 2013). Nevertheless, this strategy proved to be the most successful, even though we experienced some odd anterograde transport in one of the cases.

As separate injections seemed to give more reliable results than mixed injections, I speculate that this approach gives the AAV virus the ability to express its "payload" before the RABV is present. This way the AAV virus can secure the entire framework necessary for viral transport, in absence of the virulent nature of the RABV virus. There are however important limitations associated with the use of RABV virus itself, as it has been reported to label only a fraction of the inputs to starter cells (Callaway and Luo, 2015). The limiting factors have been related to the expression of G-protein, the number of RABV particles entering the starter cells and the time available for retrograde spread before the starter cells die (Callaway and Luo, 2015, Ghanem and Conzelmann, 2016). If it the case, it is possible that the number of inputs to the SOM cells in the LEC, reported in this thesis, is just an underrepresentation of the actual input. However, if the RABV only labels a fraction of cells, there is a possibility that the RABV virus has a preference towards some types of synaptic contacts over others, a possibility which have been speculated by others as well (Wall et al., 2013, Callaway and Luo, 2015). This could imply that my results partially reflects the RABV virus selective nature of synaptic contacts, which may have led to a biased labelling of monosynaptic inputs.

4.5 Monosynaptic inputs to somatostatin interneurons in the lateral entorhinal cortex

Monosynaptic projections to the SOM population in the LEC were found to originate in different structures throughout the entire brain. Overall, the inputs to SOM cells in the LEC seem to be closely comparable to the general input pattern reported for the LEC (Burwell and Amaral, 1998), with a few exceptions.

4.5.1 Intrinsic inputs from the lateral entorhinal cortex

The highest number of monosynaptically labeled cells was found within the LEC itself, demonstrating a strong intrinsic connectivity. In fact, more than 70% of the counted input cells from my tracing experiment were found to be intrinsic projections. Most of monosynaptic labeled cells were densely packed in the superficial layers, especially in LII. These findings are in line with a recent study that reports that SOM cells in the barrel cortex receives intrinsic input from cells situated in the superficial layers (Wall et al., 2016). The same preferential connectivity was also seen in the MEC, in a study carried out in parallel to the present (Øvsthus, 2016). Interestingly, the high intrinsic connectivity seen in the LEC was not seen in the MEC, and the majority of the input to the SOM cells in the MEC were derived from extrinsic sources (Øvsthus, 2016). These results may thus reflect a fundamental difference in the overall intrinsic connectivity of INs in the LEC and the MEC.

4.5.2 Inputs from the piriform cortex

The most prominent extrinsic input source to SOM cells in the LEC was the Pir. More than half of the extrinsic input neurons were found here. This massive Pir to LEC projection is in line with other reports that 1/3 of the cortical inputs to the LEC come from the Pir (Burwell and Amaral, 1998). In my data, 4/5 of the cortical inputs to the LEC originate in the Pir, which is more than previously reported. However, it seemed that my injection site was situated close to the border between the LEC and the Pir. We thus speculate that an unknown number of starter cells might have been situated in the Pir, and that some of the monosynaptically labeled cells reflect intrinsic connections of the Pir. Most of the rabies infected cells were located in LII, and a majority of them were identified to have a pyramidal shape, suggesting that a majority of the inputs are glutamatergic. These findings are also supported by previous reports looking at inputs to the LEC over all cell groups (Burwell and Amaral, 1998, Yang and Sun, 2015).

4.5.3 Inputs from the perirhinal cortex

A substantial amount of the monosynaptic inputs to SOM cells in the LEC arose from the PRh. This relatively strong connectivity from the PRh to the LEC has also been reported in earlier studies (Burwell and Amaral, 1998). The labeled cells were mainly confined to the superficial layers, with only a few scattered cells expressing GFP in deeper layers.

4.5.4 Inputs from the hippocampus

A relatively modest amount of projecting cells were found in the HF. Labelled cells were seen in the CA1, CA2 and the Sub. The highest number of cells were seen in the CA1. The CA2 housed a few cells, while only one cell was situated in the Sub. All three hippocampal structures have previously been reported to project to the LEC, and CA1 and the Sub are known to innervate the LEC substantially (Agster and Burwell, 2013)**.** The CA1 and the Sub inputs are also shown to terminate in the same topographical area of LEC (Witter and Amaral, 2004)**.** My results show that monosynaptic inputs to SOM cells in the LEC are relatively weak, that they mainly arise in the CA1, and that projections from the Sub are virtually non-existent. In the MEC the same input pattern from the HF was seen, and only CA1 cells were reported to project to SOM cells here (Øvsthus, 2016). These findings may imply that different neuronal subpopulations, such as the SOM cells, may preferentially receive inputs from only a restricted portion of the HF Moreover, this indicates that input to different neuronal subpopulations does not necessarily reflect the overall input pattern to an area.

4.5.5 The major subcortical inputs

The LEC has previously been reported to be strongly connected to several subcortical structures. My experiments show the SOM cells receive 8% of their total extrinsic input from subcortical areas. A few structures were particularly strongly input providers to the SOM cells. The most prominent subcortical input was from the amygdala. This relatively strong amygdaloid connectivity to the LEC is well known, and the inputs have been reported to preferentially target deeper layers (Pitkanen et al., 2000, Majak and Pitkanen, 2003). As the

amygdaloid complex was considered as one structure, I did not identify the particular nuclei were the inputs originated. However, earlier studies have reported that the basolateral complex of the amygdala is set of nuclei that innervate the LEC most strongly (Pitkanen et al., 2000).

A few traced cells were found within the MSC, which is known to send a prominent projection to the EC (Cappaert et al., 2015). Three cells were located in the HDB, two cells were situated in the MS, while one cell was found in the VDB. My results contradict earlier findings, which have suggested that the VDB is more strongly connected to the LEC than the HDB and the MS (Alonso and Kohler, 1984). Inputs from the MSC have been reported to terminate densely in deeper layers of the LEC, but some afferents have also been found to terminate in superficial layers (Alonso and Kohler, 1984). The topography or laminar distribution of the starter population may explain the skewed input reported here compared to previous studies.

The claustrum has in this thesis been subdivided into the anterior claustrum (Cl) and the dorsal endopiriform nucleus (DEn), and labelled cells were found in both structures. Earlier reports have claimed that the claustrum is the most strongly connected subcortical structure with the LEC (Park et al., 2012). This did however not seem to be the case for SOM cells in the LEC. The claustral inputs to the LEC have also been shown to preferentially terminate in the deeper layers, as most of the other subcortical inputs (Behan and Haberly, 1999).

4.5.6 Other inputs to the somatostatin cells in the lateral entorhinal cortex

Insular cortex

The insular cortex is known to be strongly connected to the LEC (Kerr et al., 2007). However, in my experiments I only located one projecting cell within the insular cortex, even though insular input is described to preferentially target deeper layers of the LEC, where the SOM cells are most abundant (Mathiasen et al., 2015). It is possible that my starter cells were located either in a lamina or a sub region of the LEC that is less strongly connected to the

insular cortex. However, according to Mathiasen, the strongest projections from to insular cortex terminates in the anterior half of the LEC, directly ventral to the rhinal fissure (Mathiasen et al., 2015), which is in close proximity to my presumed injection site. This might imply that the strong overall input from the insular cortex to the LEC is not reflected in the inputs to SOM cells.

I report that 23 different brain areas project to the SOM cells in the LEC. The major projections have been discussed above, however a number of brain areas only showed sparse projections to the LEC. These areas include the thalamus, the temporal association cortex, the somatosensory cortex, the MEC, the olfactory tubercule and the amygdostriatal transition area. In addition, two cells were seen in contralateral Pir and the somatosensory cortices. All of these areas have been reported to project to the LEC (Burwell and Amaral, 1998, Dolorfo and Amaral, 1998, Van der Werf et al., 2002, Vertes et al., 2006, Kerr et al., 2007, Cappaert et al., 2015). The weak input from the MEC was surprising, as a prominent projection has been reported from the MEC to the LEC. This could potentially also be explained by the position of my starter cells.

4.6 Functional Implications

My results from the monosynaptic tracing experiments, show that SOM cell in the LEC primarily receives input from local afferents. As ¾ of the total input seems to be derived for local sources, the SOM cells thus seem to be heavily involved in the intrinsic network of the LEC. This strong input pattern seems to reflect what has been previously been reported for SOM cells in the neocortex (Fino and Yuste, 2011). However, SOM cells in the MEC seem to stand out from this connectivity pattern, as they receive most of their inputs from extrinsic sources (Øvsthus, 2016). I do not know if the difference in SOM cell connectivity reflects a general difference related to the internal networks of the MEC and the LEC, or if it is just a feature reserved these two distinct SOM populations. However, these results may indicate that the difference seen in functional properties between the LEC and the MEC, may be related to their respective intrinsic connectivity (Deshmukh and Knierim, 2011).

In the intrinsic network of the LEC, SOM cells seems to be preferentially targeted by local cells situated in LII and III, layers reported to constitute the main projections from the LEC to the HF (Cappaert et al., 2015). SOM expressing cells have generally been associated to co-express GABA, and some studies have shown that SOM cells can contribute to lateral inhibition (figure 3C), both in the neocortex and the HF (Boyett and Buckmaster, 2001, Lee and Huguenard, 2011). As I have seen in my thesis, SOM cells in the LEC seem to share several characteristics with SOM cells situated in other parts of the (neo)cortex, with regards to their distribution and some morphological features. It thus seems reasonable to imply that their functional characteristics also could be similar. With this in mind, there is reasons to believe that SOM cells in the LEC are be a part of an inhibitory network that is targeted by LII and LIII neurons. If the inhibitory effects of SOM cells in the LEC, are similar to those reported in other brain regions, SOM cells in LEC might project back to cells in LII and III, and hence serve to increase the signal-to-noise ratio of inputs from the LEC to the HF.

4.7 Future directions

The results in this thesis revealed new information concerning the distribution and sources of monosynaptic inputs to SOM cells in the LEC. This information gave us clear indications of a resemblance between the SOM cells in the LEC and in the (neo)cortex. However, in order to fully understand the functional relevance of SOM positive neurons in the LEC, there is a need for further both morphological and electrophysiological characterization of this subpopulation of cells.

By performing viral tracing experiments I as able to identify the input sources to the SOM cells in the LEC, which indicated that the majority of the input to SOM cells arise inside the intrinsic network. However as I only had one successful case of successful viral tracing, the results are biased towards input targeting the region close to my injection site. In order to rule out any potential topographical bias from the placement of the injection, there is a need for additional viral tracing experiments targeting other regions of the LEC.

The function of (Neo) cortical micro circuits are a result of the interplay between many distinct neuronal subpopulations. As SOM cells are only one out of three major non-

overlapping subpopulations of INs in the (neo)cortex expressing different markers, a characterization of the SOM cells are not sufficient to comprehend the functional aspects of the LEC. It would thus to be interesting to perform a similar characterization of other cell types in the LEC. This way I could have obtained a deeper insight into the overall distribution and connectivity of INs in the LEC, and possibly a greater understanding of LECs micro circuitry.

5. Conclusion

In this thesis I aimed to characterize the SOM expressing cell population in the LEC. From my distribution analysis I saw that the majority of SOM cells were situated in deeper layers of the LEC, and that the SOM cells were evenly distributed throughout the dorsoventral axis. Monosynaptic inputs to the SOM cell population were identified from 23 different brain regions, however the strongest input source originated from within the LEC itself. This strong intrinsic connectivity pattern could indicate that SOM cells are strongly involved in intrinsic computations within the LEC, and one intended role might be to increase the signal-to-noise ratio of the inputs to the HF.

In addition, the Ssttm2.1 (cre)Zjh/J transgenic mouse line was found to be highly specific for SOM cells. In regards of the viral injection strategies, separate injections with an intermediate to high volume of virus seemed to be most optimal strategy for retrograde monosynaptic viral labeling.

6. References

J Neurosci.

AGSTER, K. L. & BURWELL, R. D. 2013. Hippocampal and subicular efferents and afferents of the perirhinal, postrhinal, and entorhinal cortices of the rat. *Behav Brain Res,* 254**,** 50-64.

ALONSO, A. & KOHLER, C. 1984. A study of the reciprocal connections between the septum and the entorhinal area using anterograde and retrograde axonal transport methods in the rat brain. *J Comp Neurol,* 225**,** 327-43.

AMARAL, D. G., SCHARFMAN, H. E. & LAVENEX, P. 2007. The dentate gyrus: fundamental neuroanatomical organization (dentate gyrus for dummies). *Prog Brain Res,* 163**,** 3-22.

ASCHAUER, D. F., KREUZ, S. & RUMPEL, S. 2013. Analysis of transduction efficiency, tropism and axonal transport of AAV serotypes 1, 2, 5, 6, 8 and 9 in the mouse brain. *PLoS One,* 8**,** e76310.

ASCOLI, G. A., ALONSO-NANCLARES, L., ANDERSON, S. A., BARRIONUEVO, G., BENAVIDES-PICCIONE, R., BURKHALTER, A., BUZSAKI, G., CAULI, B., DEFELIPE, J., FAIREN, A., FELDMEYER, D., FISHELL, G., FREGNAC, Y., FREUND, T. F., GARDNER, D., GARDNER, E. P., GOLDBERG, J. H., HELMSTAEDTER, M., HESTRIN, S., KARUBE, F., KISVARDAY, Z. F., LAMBOLEZ, B., LEWIS, D. A., MARIN, O., MARKRAM, H., MUNOZ, A., PACKER, A., PETERSEN, C. C., ROCKLAND, K. S., ROSSIER, J., RUDY, B., SOMOGYI, P., STAIGER, J. F., TAMAS, G., THOMSON, A. M., TOLEDO-RODRIGUEZ, M., WANG, Y., WEST, D. C. & YUSTE, R. 2008. Petilla terminology: nomenclature of features of GABAergic interneurons of the cerebral cortex. *Nat Rev Neurosci,* 9**,** 557-68.

BEHAN, M. & HABERLY, L. B. 1999. Intrinsic and efferent connections of the endopiriform nucleus in rat. *J Comp Neurol,* 408**,** 532-48.

BERGER, T. K., SILBERBERG, G., PERIN, R. & MARKRAM, H. 2010. Brief bursts self-inhibit and correlate the pyramidal network. *PLoS Biol,* 8.

BOCCARA, C. N., KJONIGSEN, L. J., HAMMER, I. M., BJAALIE, J. G., LEERGAARD, T. B. & WITTER, M. P. 2015. A three-plane architectonic atlas of the rat hippocampal region. *Hippocampus,* 25**,** 838-57.

BOYETT, J. M. & BUCKMASTER, P. S. 2001. Somatostatin-immunoreactive interneurons contribute to lateral inhibitory circuits in the dentate gyrus of control and epileptic rats. *Hippocampus,* 11**,** 418-22.

BURWELL, R. D. 2001. Borders and cytoarchitecture of the perirhinal and postrhinal cortices in the rat. *J Comp Neurol,* 437**,** 17-41.

BURWELL, R. D. & AMARAL, D. G. 1998. Cortical afferents of the perirhinal, postrhinal, and entorhinal cortices of the rat. *J Comp Neurol,* 398**,** 179-205.

BUZSAKI, G. 1984. Feed-forward inhibition in the hippocampal formation. *Prog Neurobiol,* 22**,** 131-53.

CALLAWAY, E. M. & LUO, L. 2015. Monosynaptic Circuit Tracing with Glycoprotein-Deleted Rabies Viruses. *J Neurosci,* 35**,** 8979-85.

CANTO, C. B. & WITTER, M. P. 2012a. Cellular properties of principal neurons in the rat entorhinal cortex. I. The lateral entorhinal cortex. *Hippocampus,* 22**,** 1256-76.

CANTO, C. B. & WITTER, M. P. 2012b. Cellular properties of principal neurons in the rat entorhinal cortex. II. The medial entorhinal cortex. *Hippocampus,* 22**,** 1277-99.

CANTO, C. B., WOUTERLOOD, F. G. & WITTER, M. P. 2008. What does the anatomical organization of the entorhinal cortex tell us? *Neural Plast,* 2008**,** 381243.

CAPPAERT, N. L. M., VAN STRIEN, N. M. & WITTER, M. P. 2015. Chapter 20 - Hippocampal Formation A2 - Paxinos, George. *The Rat Nervous System (Fourth Edition).* San Diego: Academic Press.

DAYA, S. & BERNS, K. I. 2008. Gene therapy using adeno-associated virus vectors. *Clin Microbiol Rev,* 21**,** 583-93.

DESHMUKH, S. S. & KNIERIM, J. J. 2011. Representation of non-spatial and spatial information in the lateral entorhinal cortex. *Front Behav Neurosci,* 5**,** 69.

DOLORFO, C. L. & AMARAL, D. G. 1998. Entorhinal cortex of the rat: organization of intrinsic connections. *J Comp Neurol,* 398**,** 49-82.
DRUGA, R. 2009. Neocortical inhibitory system. *Folia Biol (Praha),* 55**,** 201-17.
EICHENBAUM, H., YONELINAS, A. P. & RANGANATH, C. 2007. The medial temporal lobe and recognition memory. *Annu Rev Neurosci,* 30**,** 123-52.
FEDERSPIEL, M. J., BATES, P., YOUNG, J. A., VARMUS, H. E. & HUGHES, S. H. 1994. A system for tissue-specific gene targeting: transgenic mice susceptible to subgroup A avian leukosis virus-based retroviral vectors. *Proceedings of the National Academy of Sciences of the United States of America,* 91**,** 11241-11245.
FINO, E. & YUSTE, R. 2011. Dense inhibitory connectivity in neocortex. *Neuron,* 69**,** 1188-203.
FRANKLIN K. B. J., P. G. 2007. *The Mouse Brain in Stereotaxic Coordinates,* San Diego.
FYHN, M., MOLDEN, S., WITTER, M. P., MOSER, E. I. & MOSER, M. B. 2004. Spatial representation in the entorhinal cortex. *Science,* 305**,** 1258-64.
GHANEM, A. & CONZELMANN, K. K. 2016. G gene-deficient single-round rabies viruses for neuronal circuit analysis. *Virus Res,* 216**,** 41-54.
GINGER, M., HABERL, M., CONZELMANN, K. K., SCHWARZ, M. K. & FRICK, A. 2013. Revealing the secrets of neuronal circuits with recombinant rabies virus technology. *Front Neural Circuits,* 7**,** 2.
GOLGI, C., BENTIVOGLIO, M. & SWANSON, L. 2001. On the fine structure of the pes Hippocampi major (with plates XIII-XXIII). 1886. *Brain Res Bull,* 54**,** 461-83.
GRIEGER, J. C. & SAMULSKI, R. J. 2005. Adeno-associated virus as a gene therapy vector: vector development, production and clinical applications. *Adv Biochem Eng Biotechnol,* 99**,** 119-45.
GULYAS, A. I. & FREUND, T. F. 1996. Pyramidal cell dendrites are the primary targets of calbindin D28k-immunoreactive interneurons in the hippocampus. *Hippocampus,* 6**,** 525-34.
HAFTING, T., FYHN, M., MOLDEN, S., MOSER, M. B. & MOSER, E. I. 2005. Microstructure of a spatial map in the entorhinal cortex. *Nature,* 436**,** 801-6.
HU, H., CAVENDISH, J. Z. & AGMON, A. 2013. Not all that glitters is gold: off-target recombination in the somatostatin–IRES-Cre mouse line labels a subset of fast-spiking interneurons. *Frontiers in Neural Circuits,* 7**,** 195.
INSAUSTI, R., HERRERO, M. T. & WITTER, M. P. 1997. Entorhinal cortex of the rat: cytoarchitectonic subdivisions and the origin and distribution of cortical efferents. *Hippocampus,* 7**,** 146-83.
ISAACSON, J. S. & SCANZIANI, M. 2011. How inhibition shapes cortical activity. *Neuron,* 72**,** 231-43.
JIANG, X., SHEN, S., CADWELL, C. R., BERENS, P., SINZ, F., ECKER, A. S., PATEL, S. & TOLIAS, A. S. 2015. Principles of connectivity among morphologically defined cell types in adult neocortex. *Science,* 350**,** aac9462.
KERR, K. M., AGSTER, K. L., FURTAK, S. C. & BURWELL, R. D. 2007. Functional neuroanatomy of the parahippocampal region: the lateral and medial entorhinal areas. *Hippocampus,* 17**,** 697-708.
KLOOSTERMAN, F., WITTER, M. P. & VAN HAEFTEN, T. 2003. Topographical and laminar organization of subicular projections to the parahippocampal region of the rat. *J Comp Neurol,* 455**,** 156-71.
KNIERIM, J. J., NEUNUEBEL, J. P. & DESHMUKH, S. S. 2014. Functional correlates of the lateral and medial entorhinal cortex: objects, path integration and local-global reference frames. *Philos Trans R Soc Lond B Biol Sci,* 369**,** 20130369.
KOHLER, C. & CHAN-PALAY, V. 1983. Somatostatin and vasoactive intestinal polypeptide-like immunoreactive cells and terminals in the retrohippocampal region of the rat brain. *Anat Embryol (Berl),* 167**,** 151-72.
LEE, C. K. & HUGUENARD, J. R. 2011. Martinotti cells: community organizers. *Neuron,* 69**,** 1042-5.
LEE, S., HJERLING-LEFFLER, J., ZAGHA, E., FISHELL, G. & RUDY, B. 2010. The largest group of superficial neocortical GABAergic interneurons expresses ionotropic serotonin receptors. *J Neurosci,* 30**,** 16796-808.
LEWANDOSKI, M. 2001. Conditional control of gene expression in the mouse. *Nat Rev Genet,* 2**,** 743-55.

MAINS RE, E. B. 1999. The Neuropeptides. *Basic Neurochemistry: Molecular, Cellular and Medical Aspects. .* 6th edition ed.

MAJAK, K. & PITKANEN, A. 2003. Projections from the periamygdaloid cortex to the amygdaloid complex, the hippocampal formation, and the parahippocampal region: a PHA-L study in the rat. *Hippocampus,* 13**,** 922-42.

MARKRAM, H., TOLEDO-RODRIGUEZ, M., WANG, Y., GUPTA, A., SILBERBERG, G. & WU, C. 2004. Interneurons of the neocortical inhibitory system. *Nat Rev Neurosci,* 5**,** 793-807.

MATHIASEN, M. L., HANSEN, L. & WITTER, M. P. 2015. Insular projections to the parahippocampal region in the rat. *J Comp Neurol,* 523**,** 1379-98.

MAZARAKIS, N. D., AZZOUZ, M., ROHLL, J. B., ELLARD, F. M., WILKES, F. J., OLSEN, A. L., CARTER, E. E., BARBER, R. D., BABAN, D. F., KINGSMAN, S. M., KINGSMAN, A. J., O'MALLEY, K. & MITROPHANOUS, K. A. 2001. Rabies virus glycoprotein pseudotyping of lentiviral vectors enables retrograde axonal transport and access to the nervous system after peripheral delivery. *Hum Mol Genet,* 10**,** 2109-21.

MIETTINEN, M., PITKANEN, A. & MIETTINEN, R. 1997. Distribution of calretinin-immunoreactivity in the rat entorhinal cortex: coexistence with GABA. *J Comp Neurol,* 378**,** 363-78.

MORRISON, J. H., BENOIT, R., MAGISTRETTI, P. J. & BLOOM, F. E. 1983. Immunohistochemical distribution of pro-somatostatin-related peptides in cerebral cortex. *Brain Res,* 262**,** 344-51.

NABER, P. A., LOPES DA SILVA, F. H. & WITTER, M. P. 2001. Reciprocal connections between the entorhinal cortex and hippocampal fields CA1 and the subiculum are in register with the projections from CA1 to the subiculum. *Hippocampus,* 11**,** 99-104.

NAGY, A. 2000. Cre recombinase: the universal reagent for genome tailoring. *Genesis,* 26**,** 99-109.

NASSAR, M., SIMONNET, J., LOFREDI, R., COHEN, I., SAVARY, E., YANAGAWA, Y., MILES, R. & FRICKER, D. 2015. Diversity and overlap of parvalbumin and somatostatin expressing interneurons in mouse presubiculum. *Front Neural Circuits,* 9**,** 20.

O'KEEFE, J. & DOSTROVSKY, J. 1971. The hippocampus as a spatial map. Preliminary evidence from unit activity in the freely-moving rat. *Brain Res,* 34**,** 171-5.

PARK, S., TYSZKA, J. M. & ALLMAN, J. M. 2012. The Claustrum and Insula in Microcebus murinus: A High Resolution Diffusion Imaging Study. *Front Neuroanat,* 6**,** 21.

PHAN, A. 2015. *Immunohistochemical and Morpholgoical Characterization of GABAergic Cells in the Lateral Entorhinal Cortex.* Master Masters Thesis, Norwegian University of Science and Technology.

PITKANEN, A., PIKKARAINEN, M., NURMINEN, N. & YLINEN, A. 2000. Reciprocal connections between the amygdala and the hippocampal formation, perirhinal cortex, and postrhinal cortex in rat. A review. *Ann N Y Acad Sci,* 911**,** 369-91.

RUDY, B., FISHELL, G., LEE, S. & HJERLING-LEFFLER, J. 2011. Three groups of interneurons account for nearly 100% of neocortical GABAergic neurons. *Dev Neurobiol,* 71**,** 45-61.

SCHNELL, M. J., MCGETTIGAN, J. P., WIRBLICH, C. & PAPANERI, A. 2010. The cell biology of rabies virus: using stealth to reach the brain. *Nat Rev Micro,* 8**,** 51-61.

SCOVILLE, W. B. & MILNER, B. 1957. Loss of recent memory after bilateral hippocampal lesions. *J Neurol Neurosurg Psychiatry,* 20**,** 11-21.

SILBERBERG, G. & MARKRAM, H. 2007. Disynaptic inhibition between neocortical pyramidal cells mediated by Martinotti cells. *Neuron,* 53**,** 735-46.

STRANAHAN, A. M., HABERMAN, R. P. & GALLAGHER, M. 2011. Cognitive decline is associated with reduced reelin expression in the entorhinal cortex of aged rats. *Cereb Cortex,* 21**,** 392-400.

SUZUKI, N. & BEKKERS, J. M. 2006. Neural coding by two classes of principal cells in the mouse piriform cortex. *J Neurosci,* 26**,** 11938-47.

TAHVILDARI, B. & ALONSO, A. 2005. Morphological and electrophysiological properties of lateral entorhinal cortex layers II and III principal neurons. *J Comp Neurol,* 491**,** 123-40.

TAUBE, J. S. & MULLER, R. U. 1998. Comparisons of head direction cell activity in the postsubiculum and anterior thalamus of freely moving rats. *Hippocampus,* 8**,** 87-108.

TSAO, A., MOSER, M. B. & MOSER, E. I. 2013. Traces of experience in the lateral entorhinal cortex. *Curr Biol,* 23**,** 399-405.

VAN DER WERF, Y. D., WITTER, M. P. & GROENEWEGEN, H. J. 2002. The intralaminar and midline nuclei of the thalamus. Anatomical and functional evidence for participation in processes of arousal and awareness. *Brain Res Brain Res Rev,* 39**,** 107-40.

VAN STRIEN, N. M., CAPPAERT, N. L. & WITTER, M. P. 2009. The anatomy of memory: an interactive overview of the parahippocampal-hippocampal network. *Nat Rev Neurosci,* 10**,** 272-82.

VAUGHAN, D. N. & JACKSON, G. D. 2014. The piriform cortex and human focal epilepsy. *Front Neurol,* 5**,** 259.

VERTES, R. P., HOOVER, W. B., DO VALLE, A. C., SHERMAN, A. & RODRIGUEZ, J. J. 2006. Efferent projections of reuniens and rhomboid nuclei of the thalamus in the rat. *J Comp Neurol,* 499**,** 768-96.

WALL, N. R., DE LA PARRA, M., CALLAWAY, E. M. & KREITZER, A. C. 2013. Differential innervation of direct- and indirect-pathway striatal projection neurons. *Neuron,* 79**,** 347-60.

WALL, N. R., DE LA PARRA, M., SOROKIN, J. M., TANIGUCHI, H., HUANG, Z. J. & CALLAWAY, E. M. 2016. Brain-Wide Maps of Synaptic Input to Cortical Interneurons. 36**,** 4000-9.

WALL, N. R., WICKERSHAM, I. R., CETIN, A., DE LA PARRA, M. & CALLAWAY, E. M. 2010. Monosynaptic circuit tracing in vivo through Cre-dependent targeting and complementation of modified rabies virus. *Proc Natl Acad Sci U S A,* 107**,** 21848-53.

WANG, Y., GUPTA, A., TOLEDO-RODRIGUEZ, M., WU, C. Z. & MARKRAM, H. 2002. Anatomical, physiological, molecular and circuit properties of nest basket cells in the developing somatosensory cortex. *Cereb Cortex,* 12**,** 395-410.

WANG, Y., TOLEDO-RODRIGUEZ, M., GUPTA, A., WU, C., SILBERBERG, G., LUO, J. & MARKRAM, H. 2004. Anatomical, physiological and molecular properties of Martinotti cells in the somatosensory cortex of the juvenile rat. *The Journal of Physiology,* 561**,** 65-90.

WICKERSHAM, I. R., LYON, D. C., BARNARD, R. J., MORI, T., FINKE, S., CONZELMANN, K. K., YOUNG, J. A. & CALLAWAY, E. M. 2007. Monosynaptic restriction of transsynaptic tracing from single, genetically targeted neurons. *Neuron,* 53**,** 639-47.

WITTER, M. P. & AMARAL, D. G. 2004. CHAPTER 21 - Hippocampal Formation A2 - Paxinos, George. *The Rat Nervous System (THIRD EDITION).* Burlington: Academic Press.

WOUTERLOOD, F. G., HARTIG, W., BRUCKNER, G. & WITTER, M. P. 1995. Parvalbumin-immunoreactive neurons in the entorhinal cortex of the rat: localization, morphology, connectivity and ultrastructure. *J Neurocytol,* 24**,** 135-53.

WOUTERLOOD, F. G. & NEDERLOF, J. 1983. Terminations of olfactory afferents on layer II and III neurons in the entorhinal area: degeneration-Golgi-electron microscopic study in the rat. *Neurosci Lett,* 36**,** 105-10.

WOUTERLOOD, F. G. & POTHUIZEN, H. 2000. Sparse colocalization of somatostatin- and GABA-immunoreactivity in the entorhinal cortex of the rat. *Hippocampus,* 10**,** 77-86.

YANG, W. & SUN, Q. Q. 2015. Hierarchical organization of long-range circuits in the olfactory cortices. *Physiol Rep,* 3.

YUSTE, R. 2005. Origin and classification of neocortical interneurons. *Neuron,* 48**,** 524-7.

ØVSTHUS, M. 2016. *Characterization of the distribution and monosynaptic inputs to the somatostatin cell population in the medial entorhinal cortex.* Master Master thesis, Norwegian University of Science and Technology.

Appendix

Appendix I: List of animals used in experiments

List of animals:

Animal number	**Used for**	**Viral labelling**	**Injection site**
51249	Determining mouse line specificity SOM cell distribution analysis	Good viral expression	In target area
52209	Monosynaptic tracing experiment	Poor viral transport	In target area
52604	Monosynaptic tracing experiment	No viral transport	-
52607	Monosynaptic tracing experiment	No viral transport	-
52609	Monosynaptic tracing experiment	No viral transport	-
52939	Monosynaptic tracing experiment	Good viral transport	Misplaced
53048	Monosynaptic tracing experiment	No viral transport	-
53050	Monosynaptic tracing experiment	Poor viral transport	In target area
53051	Monosynaptic tracing experiment	Good viral transport	Misplaced
54793	Monosynaptic tracing experiment	Good viral transport	Misplaced
54794	Monosynaptic tracing experiment	Good viral transport	In target area

Appendix II: Surgical equipment and procedure

Surgery equipment:

- Surgery table
- Stereotaxic frame, with tower
- Induction chamber
- Heating pad
- Vaporizer unit for isoflurane
- Mask for isoflurane
- Electric razor
- Two tweezers
- Two ear bars
- Small surgery scissors
- Clamper
- Stereo microscope
- Tubes connecting the induction chamber and the mask to the vaporizer unit
- Drill (0.9 mm, Foredom Micro Motor FM3545 control and MH-145 Micro Motor Hand piece

Disposables:

- Scalpel (blade 10)
- Isoflurane
- Sterile saline
- Q-tips
- Suture kit
- Syringes
- Needles (25 and 27 gauge)
- Cotton swabs
- Ethanol
- Marcain
- Temgesic
- Rimady

Surgical procedure:

1. Clean all surfaces with 70% ethanol
2. Prepare all surgical equipment
3. Weigh the animal before surgery
4. Turn on the oxygen flow (1L/min) and isoflurane (5%). Wait for the chamber to fill up (ca 5 min)
5. Place the animal in the induction chamber and wait until the animal breaths slow and deeply
6. Shave the head of the animal with an electric razor
7. Mount the animal on the stereotaxic frame. Administer isoflurane through the stereotaxic anesthesia mask
8. Adjust the isoflurane level to 3%
9. Make sure the animal is sufficiently anesthetized by checking toe-pinch reflex
10. Perform subcutaneous injections of Rimadyl and Temgesic on the back, and subcutaneous injections of Marcain on the head.
11. Apply Simplex (Tubilux Pharma S.p.A., Italy) on the animals eyes, to prevent them from drying out
12. Fixate the skull by using ear bars, adjust the frame and make sure the ear bars are aligned
13. Clean the head with sterile saline, ethanol (80%) and iodine
14. Make an incision along the midline using a scalpel. Remove the periost one both sides of the skull
15. Use bent needles to keep the skin away from the skull
16. Adjust the position of the skull so that bregma and lambda are aligned in the horizontal plane
17. Use the drill to thin the bone along the midline in order to reveal the sagittal sinus
18. Drill a small hole to reveal the transverse sinus
19. Remove dura from the drilling site by using bent needles
20. Use the holes, together with lambda and bregma to calculate injection coordinates
21. Drill a hole in the skull at the exact injection coordinates
22. Fill up the Hamilton syringe with the desired viral tracer

23. Fasten the syringe in the stereotaxic tower
24. Adjust the needle to the stereotaxic coordinates
25. Lower the needle into the surface of the brain and do a control check of your coordinates
26. Lower the needle down to the injection site. Wait two minutes
27. Inject the virus over a time course of 10-15 minutes, depending on the volumetric size of the injection
28. After the last injection, wait 10 minutes
29. Raise the needle slowly out of the brain tissue
30. Clean the skull with sterile saline
31. Suture the wound
32. Rinse the suture with sterile saline and iodine
33. Remove the ear bars, turn off the isoflurane and remove the anesthesia mask

Post surgery procedure:

1. Place the animal in a heating chamber and wait for it to recover
2. Make a treat (i.e baby porridge) and place it in the animals home cage
3. Move the animal to its home cage
4. Monitor the animal, and make sure that it can move and eat
5. Check the animal one hour after the injection to make sure everything is normal
6. One day after surgery: Perform a subcutaneous injection of Rimadyl to relive post-surgical pain

Appendix III: Immunohistochemistry and histology protocols

Somatostatin IHC protocol:

1. Wash sections in 0.125 M PB for 3 x 15 min
2. Heat 0.125M PB to 60°C and keep the tissue in for 2h
3. Wash the sections in 0.125M PB with 1% TrX for 2 x 10 minutes for enhanced permabilization
4. Pre-incubate the sections in a blocking solution made up by 0.125 PB and 10% NGS for 3h.
5. Incubate with primary antibody, 1:500, in an incubation solution made up by 0.125 PB and 10% NGS for 48h at 4°C on a stirrer
6. Wash the sections in 0.125 M PB for 4 x 15 minutes
7. Incubate the sections with secondary antibody, 1:400, in an incubation solution made up by 0.125 M PB, 1% TrX for 24h at 4°h on a stirrer.
8. Wash the sections in 0.125 M PB for 3 x 15 minutes
9. Wash the sections in Tris-HCl (ph7.6) for 15 minutes
10. Mount the sections on microscope slides and coverslip the sections

GFP and mCherry IHC protocol:

1. Wash the sections in 0.125 M PB – 4 x 15 min
2. Incubate with primary antibody 1:500 in an incubation solution mad from 1% TrX, 0.5% DMSO, 1% Natural Goat Serum in 0.125 MPB for 48 hours at 4°C on a stirrer.
3. Wash the sections in 0.125 M PB for 6 x 15 min
4. Incubate with secondary antibody 1:500 in an incubation solution 1% Trx, 0.5% DMSO, 1% NGS in 0.125 M PB for 24 hours at 4°C on a stirrer
5. Wash the sections in 0.125M PB for 5 x 15 min
6. Wash the sections in Tris HCl (ph7.6) for 15 min
7. Mount the sections on microscope slides and coverslip the sections

HA-tag IHC protocol:

1. Wash the sections in 0.125 M PB for 3x15 minutes
2. Wash the sections in 0.125 M PB + 1% TrX for enhanced permeabilization
3. Pre-incubate sections in a blocking solution of 0.125 M PB + 1% Trx containing 5% Natural Goat Serum for 60 minutes.
4. Incubate the sections with primary antibody, 1:2000, in an incubation solution made up by 0.125 M PB + 1% Trx and 5% Natural Goat Serum for 48h at 4°C on stirrer.
5. Wash the sections in 0.125 M PB for 4 x 15 minutes
6. Incubate with secondary antibody, 1:400, in an incubation solution made up by 0.125 M PB + 1% Trx for 24h at 4°C on stirrer
7. Wash the sections in 0.125 M PB for 3 x 15 min
8. Wash the sections in Tris-HCl (ph 7.6) for 15 minutes
9. Mount the sections on microscope slides and coverslip the sections

Cresyl Violet protocol:

1. Dehydrate sections – 10 dips in each: 50-, 70-, 80-, 90-, 100-, 100-, and 100% ethanol
2. Let sections sit 2 minutes in Xylene for clearing
3. Rehydrate sections – 10 dips in each: 100-, 100-, 100-, 90-, 80-, 70-, and 50% ethanol
4. Quick wash under running water
5. Let sections sit in Cresyl Violet on shaker in dark (time depends on the age of the solution)
6. Let sections sit in running water until all excess color is washed away.
7. Move sections into the Ethanol+Acetic Acid solution for a few seconds, while you gently shake the section holder
8. Move sections quickly to a bath of cold water and let sections sit until all excess color is washed away
9. Repeat point 7) and 8) until the sections are sufficiently light, while the contrast is still good.
10. Dehydrate sections – 10 dips in each: 50-, 70-, 80-, 90-, 100-, 100-, and 100% ethanol

11. Move sections to Xylene baths for clearing. The first bath should be 2 minutes, the second should be at least 5 minutes (up to an hour).
12. Coverslip the sections with entellan in xylene.

Appendix IV: Solutions

Ringer:

0.85% NaCl (4.25 g/500 mL H_2O)

0.025% KCl (0.125 g/500 mL H_2O)

0.02% $NaHCO_3$ (0.1 g/500 mL H_2O)

Place the container with water and a magnet on a stirrer. Add the salts to the water and stir the solution until it is dissolved. Filtrate and heat to 40°C before use. Use O_2 to set the pH to 6.9 and use immediately. Fresh ringer is made before each perfusion.

Phosphate buffer (PB) 0.4M, pH 7.4:

A: $NaH_2PO_4H_2O$ 27.6 g/500 mL H_2O

B: $Na_2HPO_4H_2O$ 35.6 g/500 mL H_2O

Make solutions A and B. Add solution A to solution B until the pH is 7.4 (=0.4M). Store in a dark place at room temperature for up to a month.

Phosphate buffer (PB) 0.125M, pH 7.4:

100 mL: 31.25 mL 0.4M PB + 68.75 mL H_2O

500 mL: 156 mL 0.4M PB + 344 mL H_2O

The solution can be stored in refrigerator for up to one week.

10% paraformaldehyde (PFA):

200 mL H_2O

20 g PFA

Microwave the water to 60°C and add the measured PFA to the water. Mix the solution on a hot stirrer with a magnet and add drops of NaOH until the solution is clear. Procedure is carried out in a ventilated hood.

Fixative 4% paraformaldehyde (PFA):

200 mL 10% PFA (see above)

156 mL 0.4M PB

144 mL H_2O

Add mixed water and PB to the 10% PFA solution. Adjust the pH to 7.4 by using HCl and filtrate. Procedure is carried out in a ventilated hood. The fixative is one time use and made new for every perfusion.

Dimethyl Sulfoxide solution (DMSO):

31.25 mL 0.4M PB

46.75 mL H_2O

20 mL glycerine

Tris-HCl pH 7.6:

Tris 3.03g/500mL H_2O

Measure the water and add Tris. Adjust the pH to 7.6 with HCl.

The solution can be stored in refrigerator for up to one week.

Sucrose solution:

30g sucrose

100 mL 0.125M PB

Dissolve the sucrose in PB.

Ethanol baths used in Cresyl violet Staining:

70%: 700 mL 96% ethanol + 260 mL distilled water

80%: 500 mL 96% ethanol + 100 mL distilled water

90%: 800 mL 96% ethanol + 50 mL distilled water

Ethanol/acetic acid:

500 mL ethanol (70%)

2.5 mL acetic acid

Cresyl Violet:

0.5g Cresyl violet

500 mL H_2O

Appendix V: List of chemicals and antibodies

Primary antibodies and secondary antibodies	Manufacturer
Goat anti-somatostatin	Santa Cruz Biotechnology
Rabbit anti-green fluorescent protein (GFP)	Invitrogen
Mouse anti-mCherry	Clontech
Rat anti-HA tag	(Sigma) Roche
Normal Goat Serum	Abcam
Normal Donkey Serum	Sigma
Goat anti-mouse AF546	Invitrogen
Goat anti-rat AF488	Invitrogen
Goat anti-rat AF546	Invitrogen
Goat anti-rabbit AF 488	Invitrogen
Donkey anti-goat AF546	Invitrogen

Chemicals	Manufacturer
Acetic Acid	VWR
Cresyl Violet	Sigma-Aldrich
Dimethyl sulfoxide (DMSO)	VWR
Entellan	Merck
Ethanol	Kemetyl Norge A/S
Glycerine	VWR
Hydrogen chloride (HCl)	Merck
Paraformaldehyde	Merck
Phosphate Buffer (PB)	Merck
Potassium chloride (KCl)	Merck
Sodium chloride (NaCl)	VWR